High resolution HI observations of Messier 31

Bajaja, E.; Shane, W.W.

ASTRONOMY & ASTROPHYSICS
SUPPLEMENT SERIES

Astron. Astrophys. Suppl. Ser. **49**, 745-774 (1982)

High resolution HI observations of Messier 31

E. Bajaja (*) ([1, 3]) and W. W. Shane ([2, 3])

([1]) Instituto Argentino de Radioastronomía, Casilla de Correo No. 5, (1894) Villa Elisa (Prov. de Bs. As.), Argentina
([2]) Sterrenkundig Instituut, Katholieke Universiteit, Toernooiveld, 6525 ED Nijmegen, The Netherlands
([3]) Sterrewacht Leiden, Postbus 9513, 2300 RA Leiden, The Netherlands

Received March 3, accepted April 15, 1982

Summary. — High-resolution (24″ × 37″) observations of the central part of M31 in the 21-cm line of HI are described. The results are presented as contour maps at constant velocity and as position-velocity contour maps on a rectangular grid. Published parameters are used to construct a kinematic model for comparison with the observed data. The observed HI is attributed to two separate structures, one lying in the outer part of the disk and seen in projection against the central region as a consequence of a warp, and the other lying in the central part of the disk. This latter component is strongly concentrated in spiral arms and shows pronounced local deviations from circular motion. Arm 3 on the west side is strongly reminiscent of the 3-kpc arm in the Galaxy. Several isolated dark clouds in the central region are also observed in HI, and most of these also show deviations from circular motion, but observational limitations prevent a systematic analysis of their kinematics.

Key words : Messier 31, neutral hydrogen.

1. **Introduction.** — Because of its proximity and its favorable location on the northern sky, M31 has been the subject of several extensive surveys in the 21-cm line of neutral hydrogen. Filled aperture observations have been reported, among others, by Roberts (1966), Davies and Gottesman (1970), Gottesman and de Jager (1970), Guibert (1973) and Cram *et al.* (1980). Observations with aperture synthesis telescopes have been reported by Emerson (1974, 1976), Landecker (1978) and Unwin (1980a, b), in addition to preliminary reports on the observations described here. A more extensive survey with the same instrument is currently being executed by E. Brinks at the Leiden Observatory.

With the availability of the 8-channel line receiver for the Westerbork Synthesis Radio Telescope (WSRT) in 1971, M31 became an attractive object for investigation. Because of the prohibitive time requirements, a complete survey was deferred until a more powerful receiver should be available, and a pilot survey was initiated, restricted to a single field-center and an under-sampled velocity comb. Even with these limitations, the observations revealed a wealth of detail due to the angular resolution, which is superior to that of any other observations thus far available. The observations have been discussed previously in various contexts by Bajaja and Gergely (1977), Shane (1975, 1978) and Stark (1979), but are presented here for the first time essentially in their entirety.

Send offprint requests to : Dr. E. Bajaja, Sterrewacht, Postbus 9513, 2300 RA Leiden, The Netherlands.
(*) Member of the Carrera del Investigador Científico del Consejo Nacional de Investigaciones Científicas y Técnicas.

In the remainder of this paper we discuss the observations and the instrumental parameters (section 2), the reductions and the corrections applied (section 3), the presentation of the results in the form of contour maps (section 4), and the sources of the adopted geometric and kinematic parameters (section 5). Section 6 is devoted to a brief discussion of some of the more prominent observed features. A more systematic discussion of selected aspects will be presented separately.

2. **The observations.** — The general and mechanical features of the WSRT have been described by Baars and Hooghoudt (1974) and the 21-cm receiver system by Casse and Muller (1974). The modifications through which this receiver system was converted to an 80-channel spectrometer have been described by Allen *et al.* (1974). At the time these observations were made, the array consisted of 10 fixed telescopes, spaced at intervals of 144 meters and 2 movable telescopes which were ordinarily separated by 72 meters. In the spectrometer mode the two movable telescopes were combined with 5 of the fixed telescopes to give 10 interferometers per observation. The fixed telescopes used were either those closest to or farthest from the movable pair. In order to achieve the desired 18 meter increment in baselines, corresponding to a minimum grating ring diameter of 40′, it was necessary to observe with the movable telescopes in 4 pairs of positions, requiring 8 observations of 12 hours each for a full synthesis with interferometer baselines at 18 meter increments between 36 and 1458 meters.

The spectrometer provided 8 velocity channels, spaced

at intervals of 40 km s^{-1}. Each channel had a full width at half power of 27 km s^{-1}. In order to cover the full velocity range of M31, from − 600 to 0 km s^{-1} (heliocentric), two frequency settings were required, even without filling in the gaps between the channels, so that in total 16 12-hour observations were needed.

Most of the observations were made in July to September 1972 with a few repetitions in February 1974. Observations with missing channels or with overall phase shifts exceeding 20° were generally repeated. The nominal UV-plane coverage was very nearly complete. In the maps with velocities − 320 km s^{-1} and less, some of the longer baselines are absent during at most the first 2.5 of the observation. In the map at $V = -160$ km s^{-1} the 360 m baseline is missing until hour angle − 72.5 and five of the long baselines were inadvertently included with double weight between hour angles + 70.5 and + 72.5. The errors introduced into the maps by these flaws are expected to be well below the noise level.

At the time these observations were made, the receivers in the fixed telescopes were equipped with uncooled parametric amplifiers (Muller *et al.*, 1966) giving a system temperature of 260 K. Newly designed receivers (Allen *et al.*, 1974) had been installed in the movable telescopes giving a system temperature of 75 K. The resultant system temperature for the interferometers was 140 K (see section 3).

The single field center to be observed was placed at $\alpha = 0^h40^m.0$, $\delta = +41°03'$ (1950), about 3′ north of the nucleus. This displacement was introduced so as to help distinguish possible instrumental field-center effects from continuum radiation from the nucleus of M31. The primary beam response is 50 per cent at 19′ and 15 per cent at 30′, so that most of the visible disk of M31 along the apparent minor axis is observed but only a fraction along the major axis. The instrumental and observational parameters are summarized in table I.

3. **Data reduction and map corrections.** — Correction and calibration of the interferometric observations and transformation to the map plane were carried out with the aid of standard procedures (van Someren Gréve, 1974 ; Högbom and Brouw, 1974). Two additional corrections were required, for continuum radiation and possible frequency-independent instrumental effects, and for the short spacings which are missing from the synthesis observations. The application of these corrections is described in the following paragraphs.

In addition to line radiation, each map contains a contribution from continuum radiation and certain instrumental effects. In the observations described here, the latter were caused by slight inaccuracies in the on-line data processing and were, as nearly as could be determined, the same in all velocity channels. This was also true for the contribution from continuum radiation, except for a minor difference in the antenna pattern (i.e. the spatial frequency sampling) between the two velocity settings. Having taken account of this effect in the strongest continuum sources, a single (pseudo-) continuum map could be made and subtracted from all of the velocity channels. For this purpose the channels at $V = -600$, − 560 and 0 km s^{-1} from the same observations were used in order to include the instrumental effects along with the continuum. The first two appeared to be free from line radiation. The 0 km s^{-1} channel must contain strong galactic line radiation, but this was evidently sufficiently smoothly distributed that it contributed at most a small noise-like component due to small-scale irregularities. Determining the continuum from the outer channels in this way degrades the signal to noise ratio in the single-channel maps by only 0.87 but in the total hydrogen map, the sum of 13 velocity channels, by 0.43. In the absence of more line-free channels and in view of the instrumental corrections there seems to be no alternative to this method.

The observations were made with interferometer spacings at intervals of 18 m between 36 m and 1458 m giving, after transformation, a synthesized antenna beam of 24″ × 37″ ($\alpha \times \delta$) full width at half power. For obvious geometrical reasons the spacings 0 and 18 m could not be observed. This results in a synthesized antenna pattern in which the central peak is superimposed on an extended slightly negative region. Cleaning procedures (see, for example, Högbom, 1974) can be used to eliminate this depression, but they become progressively less reliable and more costly as the region containing radiation becomes larger. In the present case, line radiation fills a large part of the observed field in some channels, and the depression is correspondingly pronounced. For example, the average brightness temperature near the field center on the uncorrected $V = -320$ km s^{-1} map is − 5.3 K.

Reliable correction for the missing spacings requires additional data derived from independent single-dish observations. At the time this correction was applied the best available data were from the survey with the Jodrell Bank Mark I telescope (Gottesman and de Jager, 1970 ; Gottesman, 1970). The single-dish observations were made with a half-power beam-width of 14′ × 18′ and rectangular filters with widths of 40 kHz spaced at 52 kHz intervals. The resulting maps were converted to artificial Westerbork interferometer responses corresponding to the 0 m, 18 m, and 36 m spacings, using the method described by Bajaja and van Albada (1979). The longest spacing represented in the 18 m data suffered an attenuation by a factor 2 and in the 36 m data by a factor 17 on account of the finite primary beam of the Mark I telescope. The 36 m calculated response was compared with the observed Westerbork data as a check on the entire procedure, and the 0 m and 18 m were incorporated in the corrected maps. Except at $V = -400$ km s^{-1} all of the corrected maps showed residual levels, even after substantial convolution, very close to zero in the regions which appeared free from line radiation. The $V = -400$ km s^{-1} map remained significantly positive in all regions, with an average base value of about 1 K, which appeared to vary slightly over the map. No attempt was made to apply an additional empirical correction, and the consequences of this zero-level deviation are visible in some of the contour maps. The source of this trouble has not been identified.

Additional processing was required in preparing the maps for display. The standard correction for primary beam attenuation was applied (Harten, 1975). The

assumed beam was circular and of approximately gaussian form with a half-power radius of 0°.313. The r.m.s. noise, which, after correction for primary beam attenuation, increases with distance from the field center, is 1.4 K at the field center. Before correction for the continuum the figure is 1.2 K, in good agreement with the predicted value (Allen *et al.*, 1974). Integration of the central peak of the synthesized antenna pattern, as far as the first zero, shows that a brightness temperature of 1 K corresponds to a flux of 1.22 mJy per beam area. These maps are described in the following section.

In order to improve the detectability of extended objects, a second set of maps was made by convolving the above set in the north-south and east-west directions with gaussian functions such that the resulting synthesized antenna pattern was practically circular and gaussian, with a half-power width of 54″. On these maps, 1 K corresponds to 4.74 mJy per beam area. The r.m.s. noise is 0.6 K at the field center. These maps are also described in the following section. They show considerably more line radiation, but at the expense of some loss of detail. An additional convolution revealed very little new information, mainly on account of baseline uncertainties.

Relevant data on the maps are summarized in table I.

4. **Contour maps of HI.** — Contour maps of the thirteen velocity channels which show line radiation from M31 are reproduced in figure 1. Because of the very different information content of the unconvolved and the convolved maps, both are shown, the convolved maps on a smaller scale and with a greater extent. On all maps the 1950 coordinates are shown, as well as the positions of three orientation stars, marked by asterisks, most easily located in figure 3 by their (λ, β) coordinates, as defined below. The (λ, β) coordinates of the stars are (3′.8 S, 14′.9 W), (11′.6 N, 13′.0 W) and (8′.8 S, 13′.8 E). The center of M31 is marked by a cross, and the heliocentric velocity and the half-power synthesized beam are shown on each map. The plots are limited to circular regions with radii of 0°.32 and 0°.50 in order to avoid excessive crowding of contours due to noise. The contour levels on the unconvolved maps are spaced at uniform intervals of 4 K beginning at + 4 K. On the convolved maps the intervals are 2.75 K from + 2.75 K to + 16.5 K and thereafter 5.5 K.

The presence of grating rings is evident on many maps, particulary the convolved ones. For example, all of the apparent radiation on the west side of the map at $V = -200$ km s^{-1} is due to grating rings. No confusion is possible in most cases, but near the systemic velocity, where the radiation is widely distributed, there is some overlapping of grating rings from one part of the galaxy with radiation from another. Since the origin of the grating rings on these maps is always evident, no attempt has been made to delete them from the plots. Removal with the aid of a cleaning procedure would have been impractical and, in most cases, superfluous (see section 3).

The observed data are essentially completely presented in figure 1. Single channel maps, however, are very poorly suited to a discussion of the distribution and kinematics of the gas. For this purpose a second set of maps (Fig. 2) has been prepared. These are made by plotting the brightness temperature as a function of velocity and of position along a chosen line. The lines chosen for these maps describe a rectangular grid, parallel and perpendicular to the adopted line of nodes of M31. The spacing between lines is uniformly 4′.5. The coordinates are described in the rectangular (λ, β) system (see Berkhuijsen and Wielebinski, 1973) with respect to the nucleus of M31. The λ-coordinate is parallel to the line of nodes. Directions are indicated by letters (N, S, E, W) rather than by signs to avoid possible confusion between sign conventions. The position of the nucleus and the orientation of the line of nodes are taken from Baade and Arp (1964). The positions of the cross-cuts are shown in figure 3, superimposed on a blue photograph of M31.

The contour maps in figure 2 are derived from the data after convolution to the 54′ beam, in order to achieve maximum sensitivity. The contour levels are 1.5, 3, 6, 10, 15 K, and further at intervals of 5 K. No resolution element is shown because it is undefined in the velocity coordinate. The data are strongly undersampled in velocity so that, because of the necessary interpolation, the resolution element in velocity varies from 27 km s^{-1} at the velocities of the channels to more than 40 km s^{-1} half way between. The grating rings which would appear in these maps do not in general arise from radiation in the same map so that their identification is difficult. For this reason, the maps in figure 2 have been carefully edited, comparing each one with all of the single channel maps and deleting all contours which could be identified with grating rings. Because many of the maps in figure 2 extend beyond the limits of figure 1, grating ring confusion and high-amplitude noise are encountered more frequently. In cases of uncertainty, contours were not deleted, so that in all probability some of the features at the extreme ends of the cross-cuts will be unreal. A model rotation curve, described in section 5, was adopted and the expected velocity at each point on the cross-cuts was calculated. The result is plotted as a heavy broken curve. This curve will be used as a reference in the discussion of the observed kinematics in section 6.

5. **Adopted geometric and kinematic parameters.** — The observation reported here do not extend far enough along the line of nodes of M31 to yield significant new information on the complete geometry or kinematics. Nevertheless, for any interpretation of the observations, some model is required, and we have adopted one based on published data.

The position of the nucleus and the orientation of the line of nodes (identified here with the major axis, despite clear evidence of a warp) are taken from Baade and Arp (1964). The inclination (the angle between the rotation axis of M31 and the line of sight) is taken to be 77°, in agreement with several recent investigations (e.g. Cram *et al.*, 1980), and about midway between the extreme values, 74° to 79°, encountered in the recent literature.

A comparison of the single-channel maps (Fig. 1) at -280 km s^{-1}, -320 km s^{-1} and -360 km s^{-1} indicates that the systemic velocity must be between -280 km s^{-1} and -320 km s^{-1}, and that it is closer to -320 km s^{-1}. A value $V_{sys} = -310$ km s^{-1} (heliocentric) was therefore adopted. This value is well within

the range of recent determinations. The position-velocity map (Fig. 2) at $\lambda = 0$ shows a peak consistently at $V = -320$ km s^{-1}, but this is the velocity of the nearest channel, and the deviation from the adopted value is attributed to undersampling. Rotation curve data were compiled from a number of sources. Optical data were used in the innermost regions, where the 21-cm radiation is weak and beam smoothing is important. Where reliable 21-cm data were available these were used in preference to the optical results. The combination of data used in various zones in M31 is reported in table II. The data from Emerson (1976) were first approximately corrected for beam smoothing by adding 10 km s^{-1} at $r \leq 50'$ and smaller corrections at greater distances, decreasing to 0 at $r \geq 100'$. When available, data from both sides of the minor axis were averaged. Small-scale irregularities in the tabulated values were removed by smoothing. Extracts from the data from the five sources consulted are plotted in figure 4, along with the smoothed rotation curve. The large systematic difference between the radio and optical data at $r > 80'$ is not readily explained. It could be due to the concentration of the optical points, which are relatively scarce in this zone anyway, in regions with deviant velocities. The radio data, on the other hand, could be contaminated by contributions from remote regions of the galaxy as a consequence of the warp (see section 6 and Roberts *et al.,* 1978).

The reference velocity curves shown in figure 2 were calculated from a planar model with pure circular rotation, based on the parameters described here, which are summarized in table III.

6. **Discussion.** — The observations presented here, which were made as a pilot survey, contain only a small sample of what would be derived from a complete survey with the Westerbork telescope. In particular, they are restricted to a relatively small region centered about 3′ north of the nucleus (see Fig. 3) and are undersampled in velocity, where the interval between maps is 40 km s^{-1} whereas the bandwidth, because of instrumental limitations, was 27 km s^{-1}. This results in uncertainties of up to 50 per cent in estimates of column densities in individual narrow features. The influence on the general density field is much less. Another result of the undersampling is seen in figure 2, where the highest brightness temperatures appear to lie at the observed velocities (see, for example, figure 2, $\beta = 13.5$ W). From these same maps it appears also that the column density reaches a peak where the profile is centered on an observed velocity and a minimum where it is centered between two channels.

Despite these limitations, a good deal can be learned from an inspection of figures 1 and 2 and the results derived from them. Bajaja and Gergely (1977) have used the HI column densities in connection with a discussion of the optical absorption. These results have been reported in full and need not be enlarged upon here. Shane (1978) took brief note of some kinematical results, which will be discussed further here, and some remarks will be added on the HI distribution and its correlation with optical features.

As was noted by Bajaja (see Shane, 1975), there are extended regions in which the line profiles appear to be double-peaked. These are seen most clearly in figure 2 and offer an important key to the problem of the HI distribution. We note the existence of two HI components, one lying quite close (in most cases) to the velocity derived from the adopted rotation curve and the other lying much closer to the systemic velocity. Comparison with a photograph shows that the first, or « high velocity », component coincides with the spiral arms, in particular the dust lanes, and is absent elsewhere, whereas the « low velocity » component shows no correlation with the spiral structure and is quite widely and smoothly distributed. The two components, when present, will be resolved in these observations when their velocities differ by more than 80 km s^{-1}. Examples of this are seen in figure 2 in parts of the cross-cuts at $\beta = 4.5$ W, 0.0 and 4.5 E and at $\lambda = 18.0$ S, 18.0 N, 22.5 N and 27.0 N. The differences reflect differences in the global rotation properties and are enhanced in some regions by local velocity peculiarities. For example, at $\lambda = 9.0$ N the high velocity component shows a large velocity deviation from the value derived from the adopted rotation curve. Such deviations could indicate the presence of local peculiar motions in the plane of M31, but they might also be explained in part by inaccuracies in the adopted rotation curve or by a warp in the disk of M31. That radial motions in the disk do play an important role is seen unambiguously at $\lambda = 0.0$ west of the nucleus, where the deviations from the systemic velocity coincide in position with spiral arms 3 and 4 (Baade's nomenclature) and an optically indistinct inner feature. Stark (1979) finds the same velocity deviations at the same positions in CO observations and virtually nothing at the systemic velocity, indicating that the deviant velocities are associated with the spiral arm density maxima. Figure 2 ($\beta = 4.5$ W) shows that deviant velocity gas at $\lambda = 0.0$ is associated with the high velocity component and systemic velocity gas with the low velocity component. A similar separation into two components can also been seen on the east side of the line of nodes, at $\lambda = 18.0$ S, 13.5 S, 22.5 N and 27.0 N, but it is less distinct for three reasons. The spiral arms are less well resolved in HI on the east, or far, side than on the west where a warp in the disk apparently produces a more favorable projection. The spiral arms show no large deviations from circular rotation on the east side, so that the components are completely blended at $\lambda = 0.0$. Finally, the low velocity component is weaker on the east side than on the west.

Both components require further discussion. The low velocity component is most readily interpreted as being located far from the center of M31. The velocity gradient of this component derived from figure 2 ($\beta = 4.5$ W, where it is most clearly resolved) is about 2.7 km s^{-1} arcmin.$^{-1}$. This is reproduced from the adopted rotation curve (Fig. 4) if the gas is located about 17 kpc from the nucleus. To place this gas in the line of sight requires that it be about 3 kpc from the plane of M31, in agreement with the estimate of Whitehurst *et al.* (1978). Our observations do not indicate whether we should interpret this as a broadening of the HI layer in these regions or a warp in the layer. It is seen in most of the constant-λ cross-sections (Fig. 2) on both sides of the line of nodes, although often more strongly on the west side. If this is to

be interpreted as a series of rings beginning between 10 and 15 kpc from the center and tilted with respect to the inner disk, then the tilt angle must increase outward to about 13° around an axis roughly coincident with the line of nodes. Mainly on account of the limited velocity sampling the two components begin to blend beyond 5′ from the line of nodes, although a broadening with increase distance from the minor axis is still noticeable at β = 9.0 E and 9.0 W.

A similar splitting into two components is seen in the data of Cram *et al.* (1980), most prominently at $\beta = -9.0$ and + 9.0. This led Whitehurst *et al.* (1978) to propose a thickening or warp in the HI layer. The two sets of observations are complemenary and lead to the same conclusion, but there is very little opportunity for direct comparison. The splitting seen by Cram *et al.* (1980) lies largely outside the field observed by us. Within that field the angular scale over which large velocity variations take place is too small for the resolution of the 100 m telescope.

In those regions west of the line of nodes where the two components are sufficiently well separated in velocity, the brightness temperature, and thus presumably the column density, of the low velocity component is slightly less than the peak value in arm 3 but more than the average in the inner disk. Because of the uncertain geometry this result cannot be simply translated into volume or surface densities.

The high velocity component is spatially associated with the spiral arms and therefore presumably quite close to the plane of M31, at least in the inner region. Thus the velocity deviations from the model predictions, particularly at $\lambda = 0.0$ and west of the line of nodes where they are most distinct, indicate real deviations from circular rotation. These are most evident in arm 3 and are illustrated in figure 5, which shows a schematic deprojected view of arm 3 on the west side of the line of nodes. The location of the arm is derived from the intensity peak of the high velocity component, and the deprojection is carried out using the parameters from table III. The arrows show the line-of-sight projections of the differences in velocity from the model predictions. From the southernmost limit of the observed field to a point 8′ north of the minor axis these differences become steadily more negative, reaching an extreme value of -70 km s^{-1}. Northward of this point the observed velocities are in agreement with the model. A unique velocity model cannot be derived from the line-of-sight components alone, but these components can be simply represented by a model in which the arm southward of the point 8′ north has an inward velocity of 30 km s^{-1} (in agreement with the measured value at $\lambda = 0.0$) and an excess rotation velocity above the adopted rotation curve (which is weakly determined in this region) of 40 km s^{-1}. Similarly, arm 4 on the west side shows an outward velocity of 20 km s^{-1} and no pronounced variation along the arm, while the indistinct inner feature has an outward velocity of 70 km s^{-1} at $\lambda = 0.0$. The inward motion, associated here with arm 3, was also noted by Cram *et al.* (1980), who also found a corresponding inward motion east of the line of nodes which we cannot identify.

The resemblance of arm 3 to the 3-kpc arm in the Galaxy is worthy of comment. Both lie at about 4 kpc from the nucleus and appear sharply defined. Both show pronounced radial motions of similar magnitude (but opposite sign). In both cases these radial motions are not symmetric but seem to be confined to about one quadrant. Whatever the origin of these peculiar motions, it is tempting to look for the same explanation in both cases.

Several explanations of the radial motions of arms 3 and 4 have been suggested. Shane (1978) noted that the radial motions could be formally accounted for by an explosion in the nucleus about 3×10^7 years ago. The nature of the explosion and the means by which momentum is transported over 5 kpc remain unclear. The 3 kpc arm in the Galaxy is frequently identified with an inner Lindblad resonance. This explanation is less attractive in the case of M31 because of the lack of symmetry. This can be attributed in the 3-kpc arm in HI, but not in CO (Bania, 1980), to masking by nearby HI (Shane, 1972). The change in position angle of the isophotal major axis of the M31 with decreasing radius observed by Peterson *et al.* (1977) could be attributed to a triaxial mass concentration (a bar). The presence of a dynamically significant bar could account for radial motions of the observed magnitude in the inner region of M31 but not, in any simple way, for the east-west asymmetry. Bertin *et al.* (1977, see also Bertin and Mark, 1978) have proposed a superposition of one- and two-arm spiral modes which can represent the kinematics, but this suggestion can only be evaluated on the basis of a detailed survey of the entire Galaxy. Byrd (1977) has suggested, on the basis of the survey of Cram *et al.* (1980), that the peculiar velocities may be accounted for by a recent passage of M32 through the disk of M31. E. Brinks (unpublished report, 1978) finds that both the high velocity and the low velocity components in the neighbourhood of arm 3 are well represented by Byrd's model. This is significant because these features were not well resolved in the observations used by Byrd, and his model was constructed mainly on the basis of line profiles from other regions. It does not appear possible on the basis of these observations to choose between these alternatives or to eliminate the possibility that other more attractive explanations of the radial motions may be offered.

Except for a number of isolated clouds (which may nevertheless be concentrations in inner spiral arms), little HI is seen closer to the center of M31 than arm 3, at about 4.5 kpc. Judging from the contour maps in figure 1 and particularly figure 2, most of these clouds have radial velocities which deviate substantially from the model predictions. In order to examine these clouds further, a list of all clouds from the catalog of Hodge (1980) within 4 kpc of the nucleus was made and is reproduced in table IV. In addition to the cloud number we give the (λ, β) position in our coordinates and the distance from the nucleus, R, and the expected radial velocity, V_E, both calculated from the model described above. The HI surface density, N_H, was determined at the position of each cloud, and when this is not less than 5×10^{20} cm^{-2} both it and the weighted mean HI radial velocity, V_H, are also listed. Presumably the dust clouds belong to the high velocity component, as discussed above, but the presence

of both components in many of the line profiles causes the values of V_H and N_H in table IV not to be representative, in many cases, of the dust cloud alone. Cloud 573, for example, is the weak feature inward of arm 3. In figure 2 ($\lambda = 0.0$) we find a velocity for this cloud of -380 km s^{-1} whereas the mean velocity, V_H, is -340 km s^{-1} due to blending with the low-velocity component at -310 km s^{-1}. A whole string of clouds, the strongest of which is number 588, is located on the inner edge of arm 3, and most of these are superimposed upon the low-velocity component (see figure 2, $\beta = 4.5$ W). Clouds 631, 638 and 644 form a complex with excess positive velocity (see figure 2, $\lambda = 9.0$ N), but all three profiles show peaks at lower velocities as well. The peak at $\lambda = 4.5$ N, $\beta = 4.5$ E, $V = -400$ may be associated with clouds 649 and 651, but the profiles at the cloud positions were too weak to give reliable results. In general, we must conclude that, although the clouds in the inner part of M31 seem to share the peculiar motions encountered in arm 3, these observations are of insufficient sensitivity and velocity resolution to permit a systematic investigation.

Some smaller clouds even closer to the nucleus have been investigated by Gallagher and Hunter (1981). Gallagher (private communication) has estimated the mass of the cloud designated D 395 as $10^4\ M_\odot$ on the basis of extinction measurements. This is well below the detection limit for HI, so it is not surprising that this and other such clouds have not yet been seen.

Acknowledgments. — We are grateful to Prof. H. van der Laan for his continued interest, to Dr. J. S. Gallagher for information on the dust clouds and to Prof. Dr. J. H. Oort and an anonymous referee for many helpful comments. The participation of E. Bajaja was made possible through fellowships provided by the Consejo Nacional de Investigaciones Científicas y Técnicas of Argentina and the Netherlands Foundation for Radio Astronomy. The Westerbork Synthesis Radio Telescope is operated by the Netherlands Foundation for Radio Astronomy (S.R.Z.M.), with the financial support of the Netherlands Organization for the Advancement of Pure Research (Z.W.O.).

References

ALLEN, R. J., HAMAKER, J. P., WELLINGTON, K. J. : 1974, *Astron. Astrophys.* **31,** 71.
BAADE, W. : 1958, *Stellar Populations* (Richerche Astronomiche, Specola Astronomica Vaticana), ed. D. J. K. O'Connell, S.J., 5, p. 3.
BAADE, W., ARP, H. : 1964, *Astrophys. J.* **139,** 1027.
BAARS, J. W. M., HOOGHOUDT, B. G. : 1974, *Astron. Astrophys.* **31,** 323.
BAJAJA, E., VAN ALBADA, G. D. : 1979, *Astron. Astrophys.* **75,** 251.
BAJAJA, E., GERGELY, T. E. : 1977, *Astron. Astrophys.* **61,** 229.
BANIA, T. M. : 1980, *Astrophys. J.* **242,** 95.
BERKHUIJSEN, E. M., WIELEBINSKI, R. : 1973, *Astrophys. Lett.* **13,** 169.
BERTIN, G., LAU, Y. Y., LIN, C. C., MARK, J. W.-K., SUGIYAMA, L. : 1977, *Proc. Nat. Acad. Sci.* **74,** 4729.
BERTIN, G., MARK, J. W.-K. : 1978, *Astron. Astrophys.* **64,** 389.
BYRD, G. G. : 1977, *Astrophys. J.* **218,** 86.
CASSE, J. L., MULLER, C. A. : 1974, *Astron. Astrophys.* **31,** 333.
CRAM, T. R., ROBERTS, M. S., WHITEHURST, R. N. : 1980, *Astron. Astrophys. Suppl. Ser.* **40,** 215.
DAVIES, R. D., GOTTESMAN, S. T. : 1970, *Mon. Not. Roy. Astron. Soc.* **149,** 237.
DEHARVENG, J. M., PELLET, A. : 1975, *Astron. Astrophys.* **38,** 15.
EMERSON, D. T. : 1974, *Mon. Not. Roy. Astron. Soc.* **169,** 607.
EMERSON, D. T. : 1976, *Mon. Not. Roy. Astron. Soc.* **176,** 321.
GALLAGHER, J. S., HUNTER, D. A. : 1981, *Astron. J.* **86,** 1312.
GOTTESMAN, S. T. : 1970, *Mem. Roy. Astron. Soc.* **74,** 73.
GOTTESMAN, S. T., DE JAGER, G. : 1970, *Mem. Roy. Astron. Soc.* **74,** 67.
GUIBERT, J. : 1973, *Astron. Astrophys. Suppl. Ser.* **12,** 263.
HARTEN, R. H. : 1975, Netherlands Foundation for Radio Astronomy, Internal Technical Report number 135.
HODGE, P. W. : 1980, *Astron. J.* **85,** 376.
HÖGBOM, J. A. : 1974, *Astron. Astrophys. Suppl. Ser.* **15,** 417.
HÖGBOM, J. A., BROUW, W. N. : 1974, *Astron. Astrophys.* **33,** 289.
LANDECKER, T. : 1978, *Structure and Properties of Nearby Galaxies* (I.A.U. Symp. No. 77), eds. E. M. Berkhuijsen and R. Wielebinski, p. 173.
MULLER, C. A., RAIMOND, E., SCHWARZ, U. J., TOLBERT, C. R. : 1966, *Bull. Astr. Inst. Netherlands Suppl.* **1,** 213.
PETERSON, C. J., FORD, W. K. Jr., RUBIN, V. C. : 1977, *Astron. J.* **82,** 32.
ROBERTS, M. S. : 1966, *Astrophys. J.* **144,** 639.
ROBERTS, M. S., WHITEHURST, R. N., CRAM, T. R. : 1978, *Structure and Properties of Nearby Galaxies* (I.A.U. Symp. no. 77), eds. E. M. Berkhuijsen and R. Wielebinski, p. 169.
RUBIN, V. C., FORD, W. K. Jr. : 1970, *Astrophys. J.* **159,** 379.
SHANE, W. W. : 1972, *Astron. Astrophys.* **16,** 118.
SHANE, W. W. : 1975, *La dynamique des galaxies spirales* (Colloque International C.N.R.S. no. 241), ed. L. Weliachew, p. 257.
SHANE, W. W. : 1978, *Structure and Properties of Nearby Galaxies* (I.A.U. Symp. no. 77), eds. E. M. Berkhuijsen and R. Wielebinski, p. 180.

VAN SOMEREN GRÉVE, H. W. : 1974, *Astron. Astrophys. Suppl. Ser.* **15**, 343.
STARK, A. A. : 1979, Dissertation, Princeton University.
UNWIN, S. C. : 1980, *Mon. Not. Roy. Astron. Soc.* **190**, 551.
UNWIN, S. C. : 1980, *Mon. Not. Roy. Astron. Soc.* **192**, 243.
WHITEHURST, R. N., ROBERTS, M. S., CRAM, T. R. : 1978, *Structure and Properties of Nearby Galaxies* (I.A.U. Symp. no. 77), eds. E. M. Berkhuijsen and R. Wielebinski, p. 175.

TABLE I. — *Observation and map data.*

Observation and map data.

Field center: α (1950)	$0^h40^m.0$
δ (1950)	$+41^\circ03'$
Primary HPBW	$0^\circ.626$
Interferometer spacings	36 (18) 1458 m
Spacings from single dish	0,18 m
Velocities (heliocentric)	-600 (40) 0 km s^{-1}
Half-power velocity channel width	27 km s^{-1}
System temperature	140 K
Radius of first grating ring	$40'.5 \times 61'.6$
Unconvolved maps:	
Synthesized HPBW	24" x 37"
Flux equivalent of 1K	1.22 mJy/beam
r.m.s. noise at field center	1.4 K
Convolved maps:	
Synthesized HPBW	54"x 54"
Flux equivalent of 1 K	4.74 mJy/beam
r.m.s. niose at field center	0.6 K

TABLE II. — *Rotation curve data.*

Rotation curve data.

Zone		Source
r = 15'	to 20'	DP
25	30	DP, RF*
35	75	DP, RF, EC
80	85	EC
90	130	2EC, GD, RWC
135	150	2E, GD

Sources:

DP	Deharveng and Pellet (1975)
E	Emerson (1976)
EC	E corrected for beam smoothing
2E or 2EC	E or EC included with double weight
GD	Gottesman and Davies (1970)
RF	Rubin and Ford (1970)
RWC	Roberts et al. (1978)

* RF was included in the mean at r = 25', but smoothing brought the curve into coincidence with DP.

TABLE III. — *Geometric and kinematic parameters.*

Geometric and kinematic parameters.

Center α (1950.0)	$0^h40^m00^s.28$
δ (1950.0)	$+40^\circ59'42''.9$
Line of nodes: θ (1950.0)	$37^\circ46'.6$
Inclination:	77°
Systemic velocity:	-310 km s^{-1} (hel.)
Rotation curve:	see figure 4

TABLE IV. — *Dust clouds near the nucleus of M31.*

Dust clouds near the nucleus of M31.

number	λ arc min	β arc min	R kpc	V_E km s^{-1}	V_H km s^{-1}	N_H $10^{20}cm^{-2}$
534	8.2 S	0.9 W	1.8	-434	-391	8
542	3.1 S	4.1 W	3.7	-347	-332	9
553	4.9 S	1.5 W	1.7	-384		
570	2.3 S	1.4 W	1.3	-344		
572	7.7 S	3.0 W	3.1	-412	-421	8
573	0.2 S	3.1 W	2.8	-307	-340	10
576	1.2 N	3.4 W	3.1	-294	-292	6
579	6.6 S	2.9 E	2.9	-400		
588	3.2 N	4.2 W	3.8	-273	-250	22
590	2.8 S	4.2 E	4.0	-386	-455	9
591	1.1 N	1.9 W	1.7	-293	-302	10
593	2.8 N	3.0 W	2.7	-270	-274	15
596	2.6 S	1.4 E	1.4	-352		
597	4.5 N	4.1 W	3.7	-257	-291	9
600	4.0 N	3.2 W	2.9	-256	-216	15
602	4.9 N	3.6 W	3.4	-249	-192	10
604	0.7 S	0.7 E	0.6	-320	-369	6
605	3.7 S	3.3 E	3.0	-360		
606	5.8 N	4.1 W	3.8	-243	-190	12
616	4.0 N	1.5 W	1.6	-250		
618	2.9 S	4.3 E	3.9	-343	-411	5
620	2.0 S	3.8 E	3.4	-335	-348	7
621	1.1 S	3.4 E	3.0	-325	-350	5
622	2.1 N	0.9 E	0.9	-279		
628	3.4 N	1.1 E	1.2	-258		
631	7.8 N	1.4 W	2.0	-191	-194	5
635	1.6 N	3.6 E	3.3	-289	-342	8
636	3.2 N	2.4 E	2.2	-262	-254	7
638	11.2 N	3.6 W	3.9	-182	-202	13
644	9.9 N	2.0 W	2.7	-170	-166	10
649	4.0 N	3.4 E	3.2	-258		
651	4.9 N	3.0 E	2.8	-241		
652	7.3 N	1.2 E	1.8	-200		
656	9.5 N	0.7 E	2.0	-168		
657	7.1 N	2.5 E	2.6	-208	-234	6
660	8.1 N	2.2 E	2.5	-192	-248	10

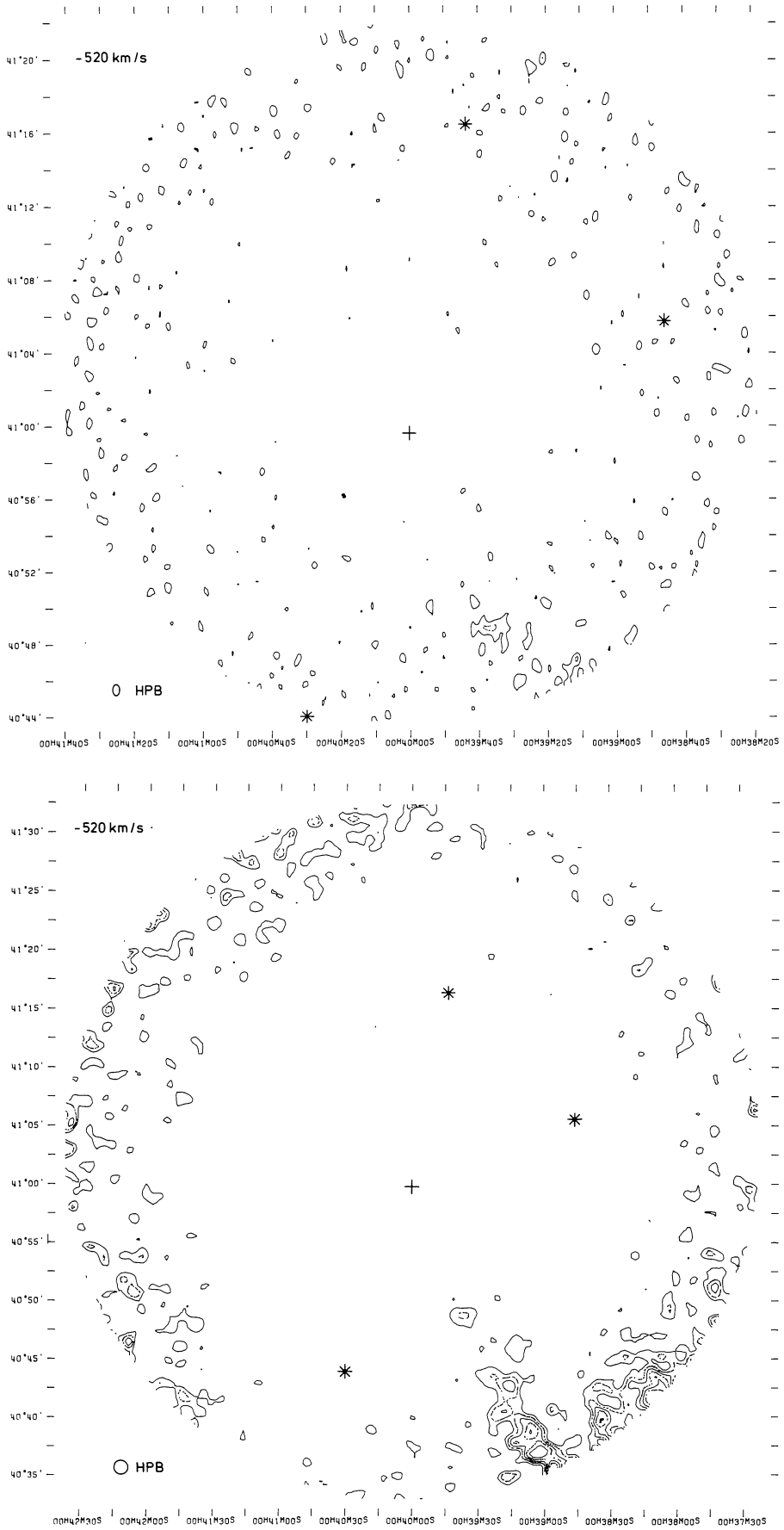

FIGURE 1. — Maps of 21-cm line brightness temperature distributions at individual velocities, as described in section 4. The upper panels show the maps at full resolution, 24″ × 37″ HPBW, and the lower panels after convolution to a 54″ HPBW circular beam.

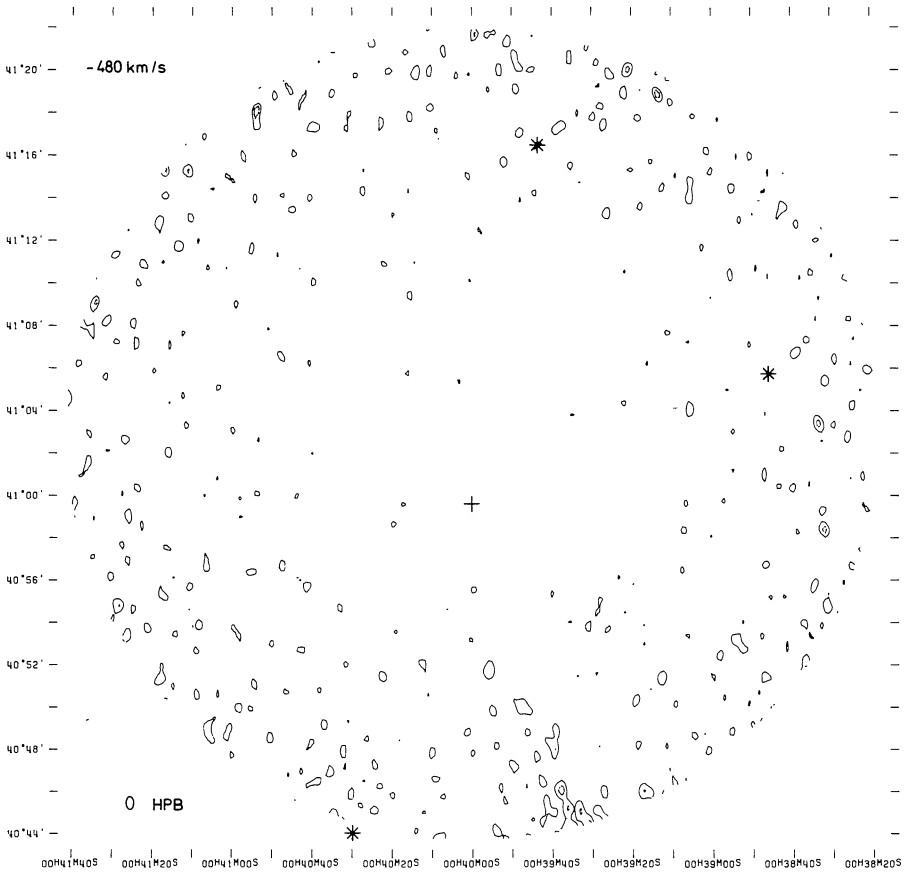

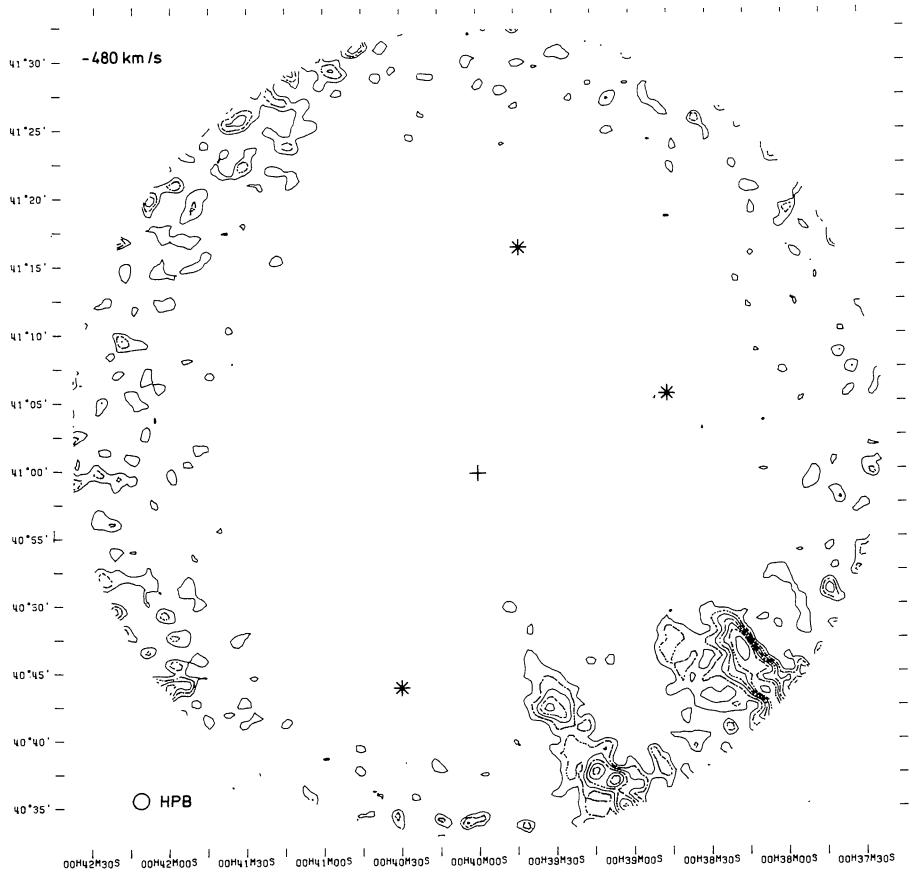

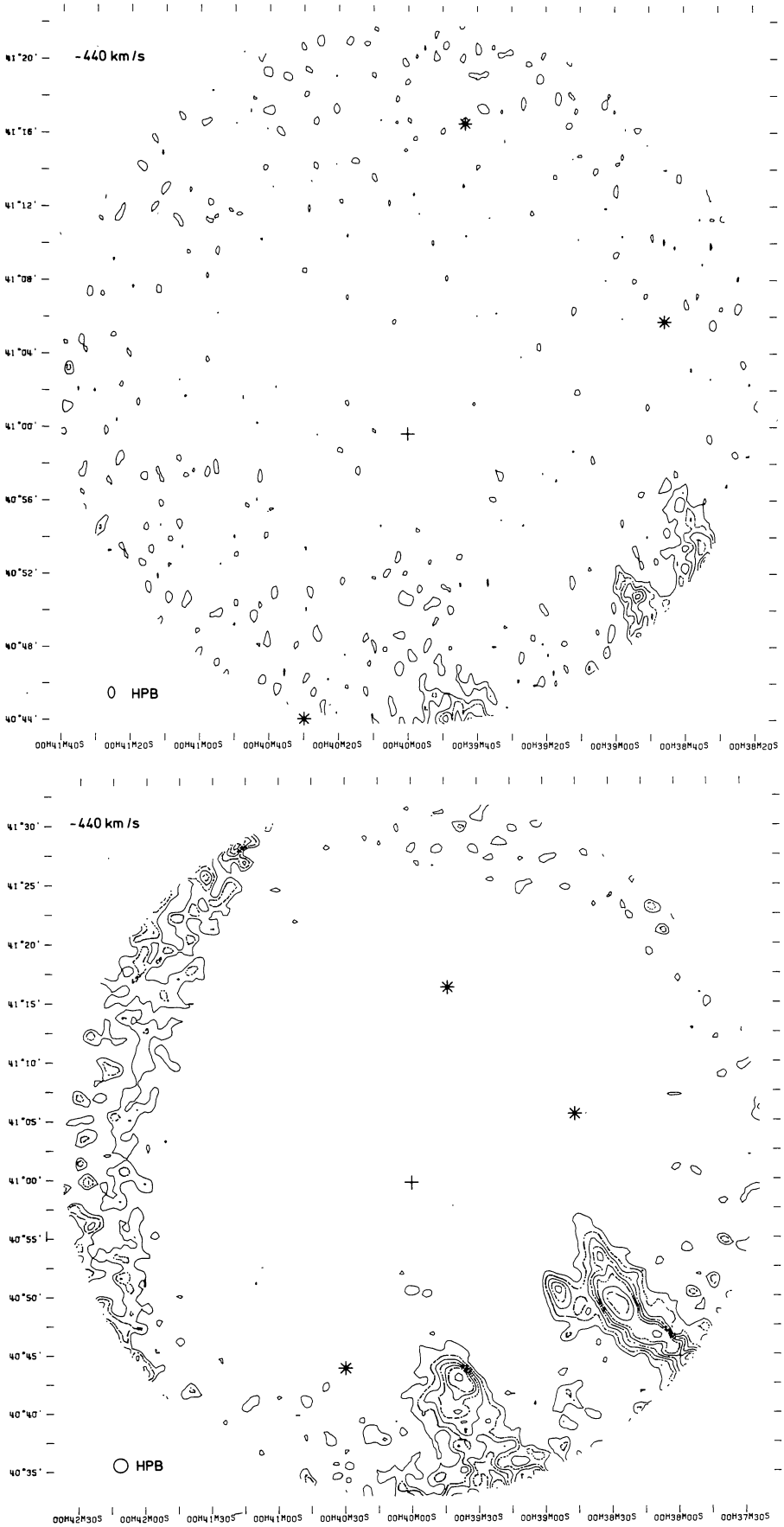

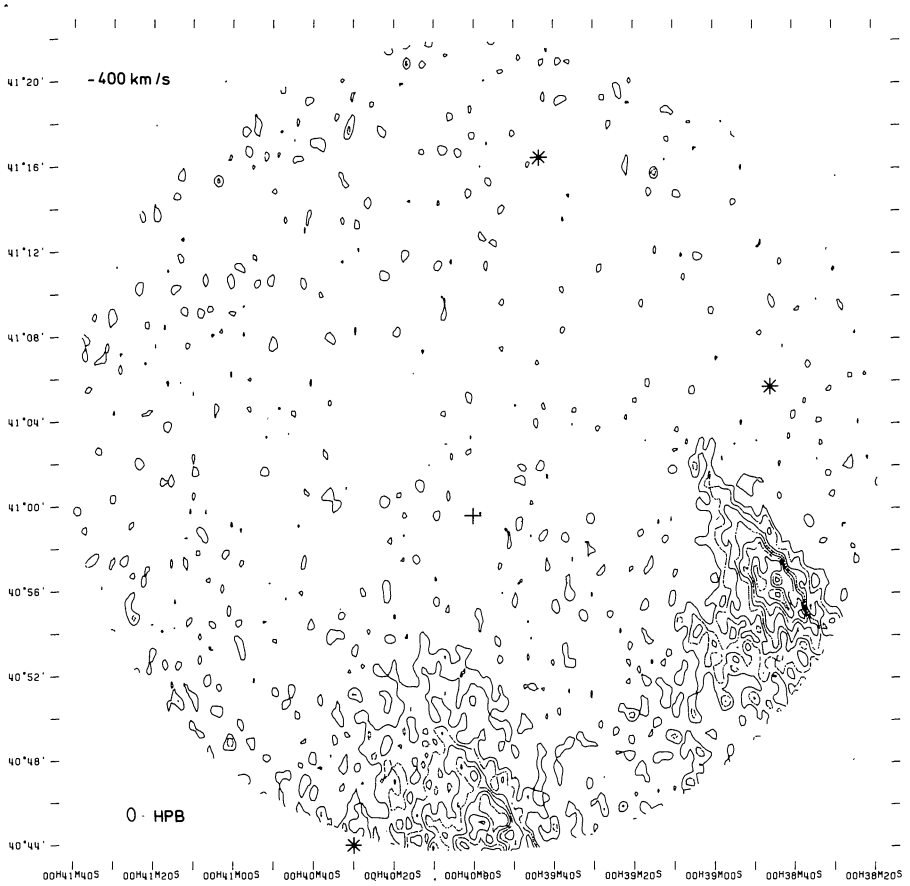

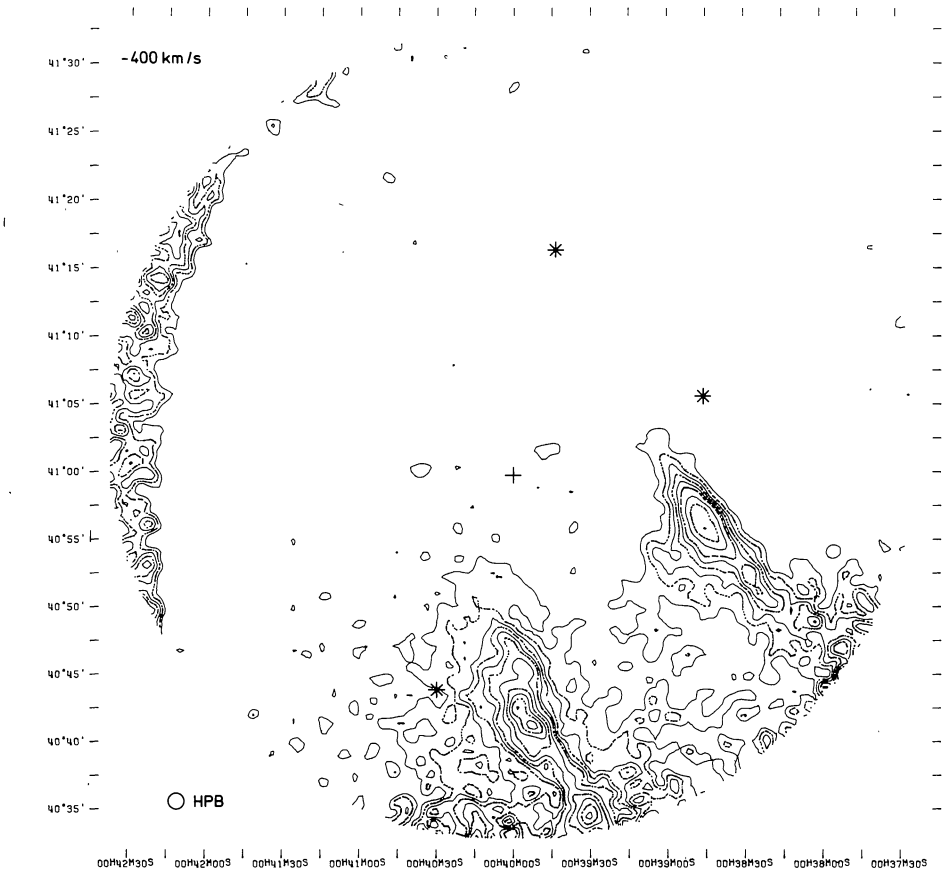

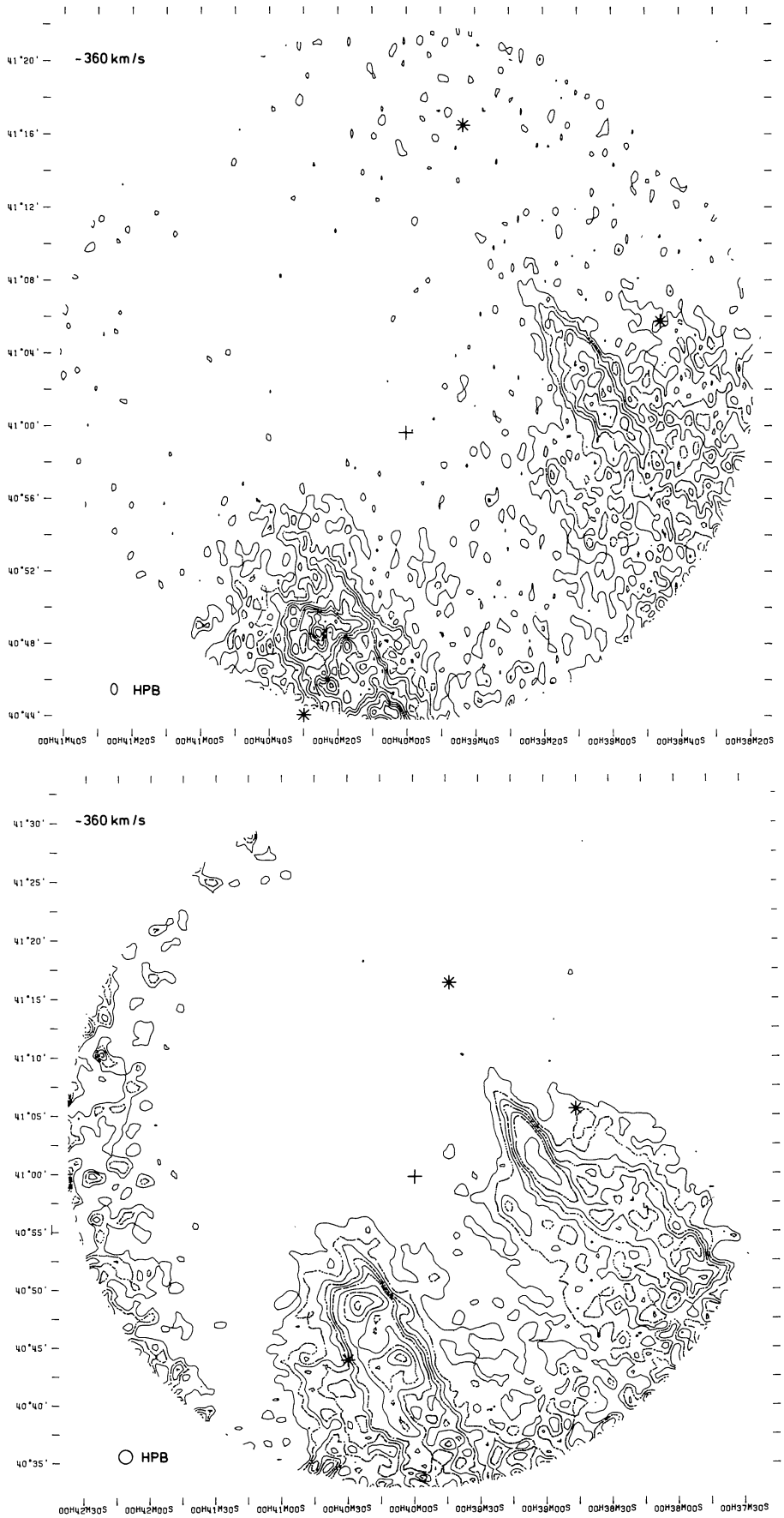

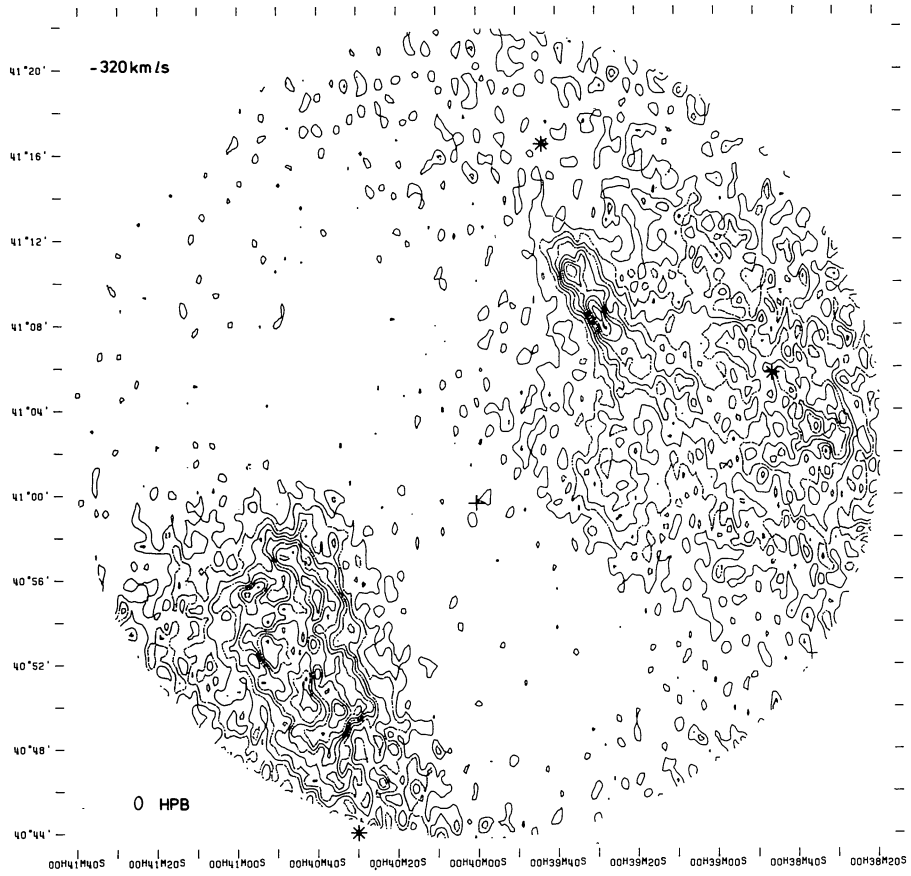

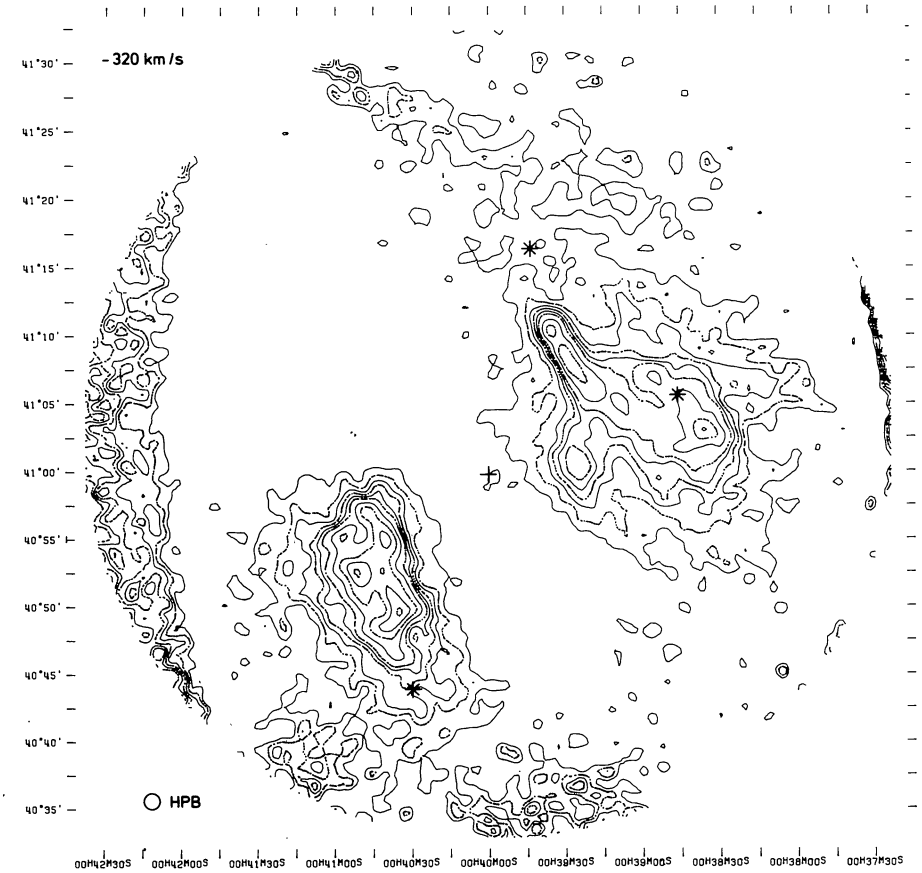

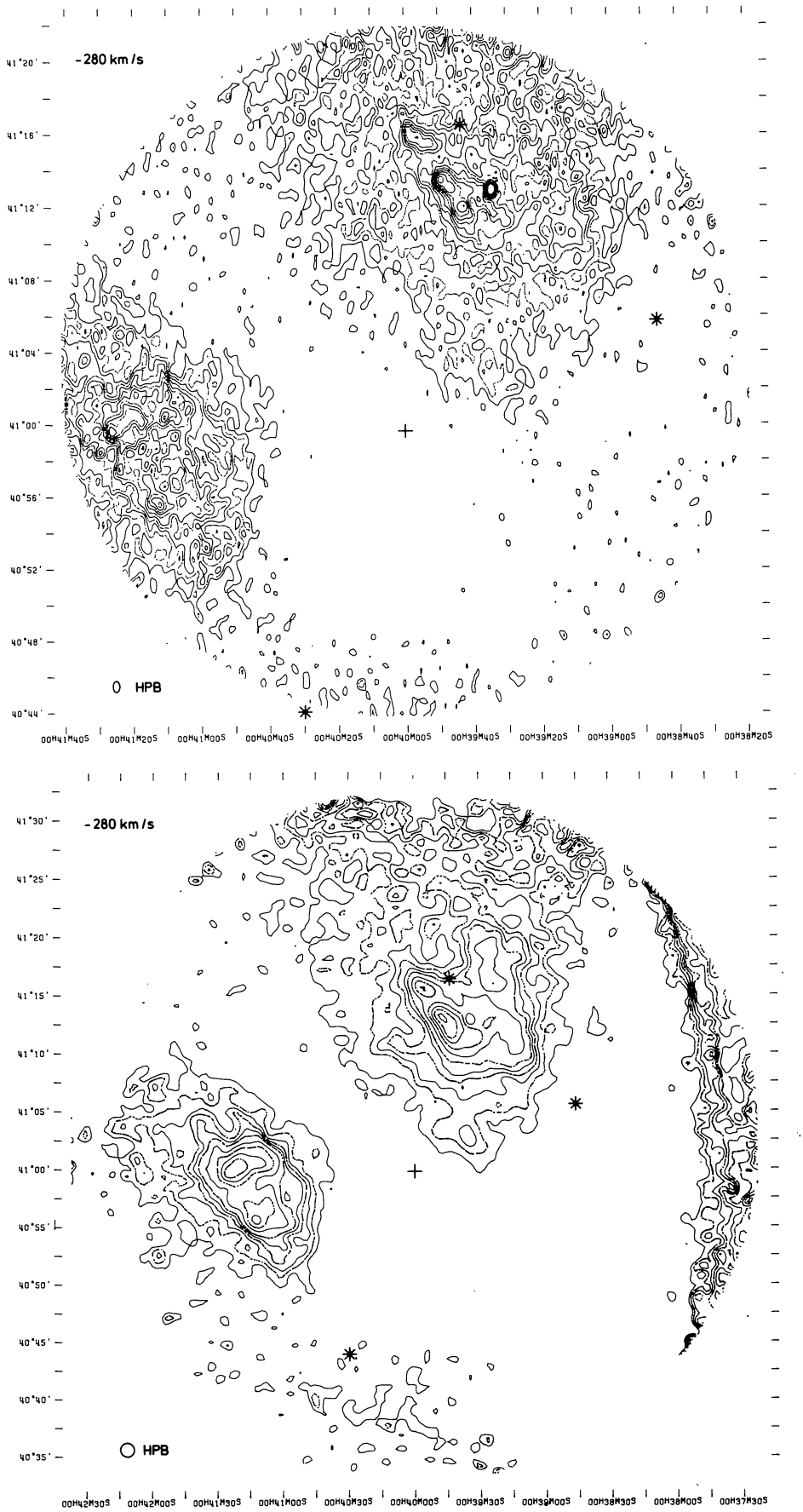

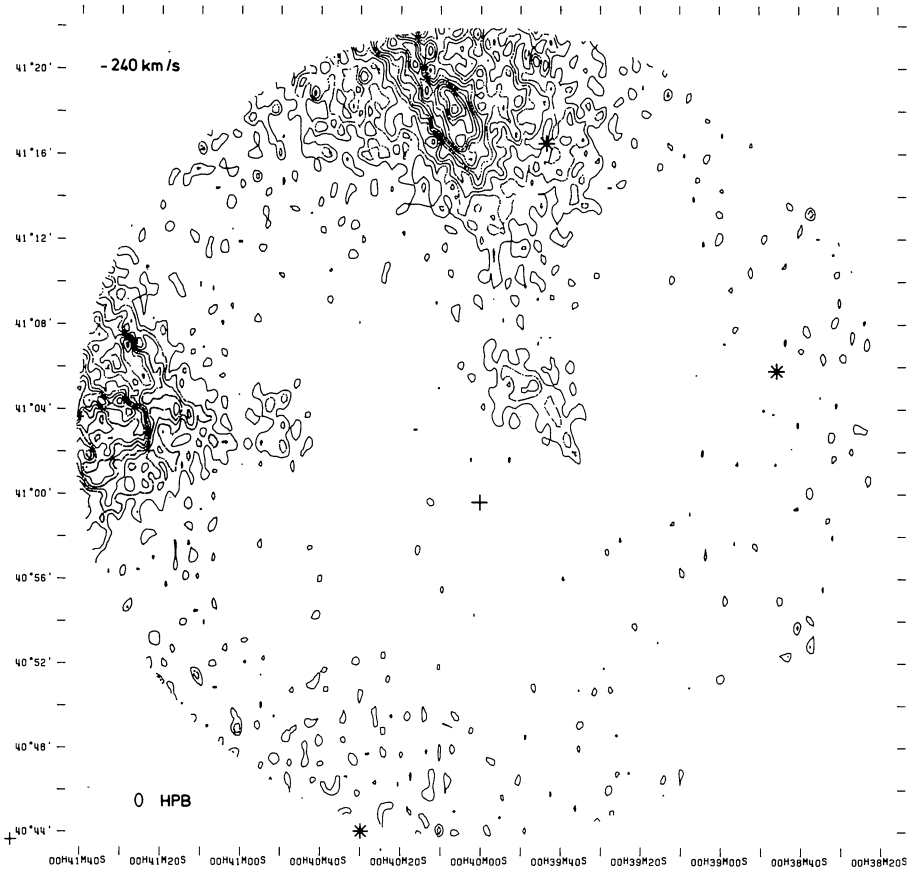

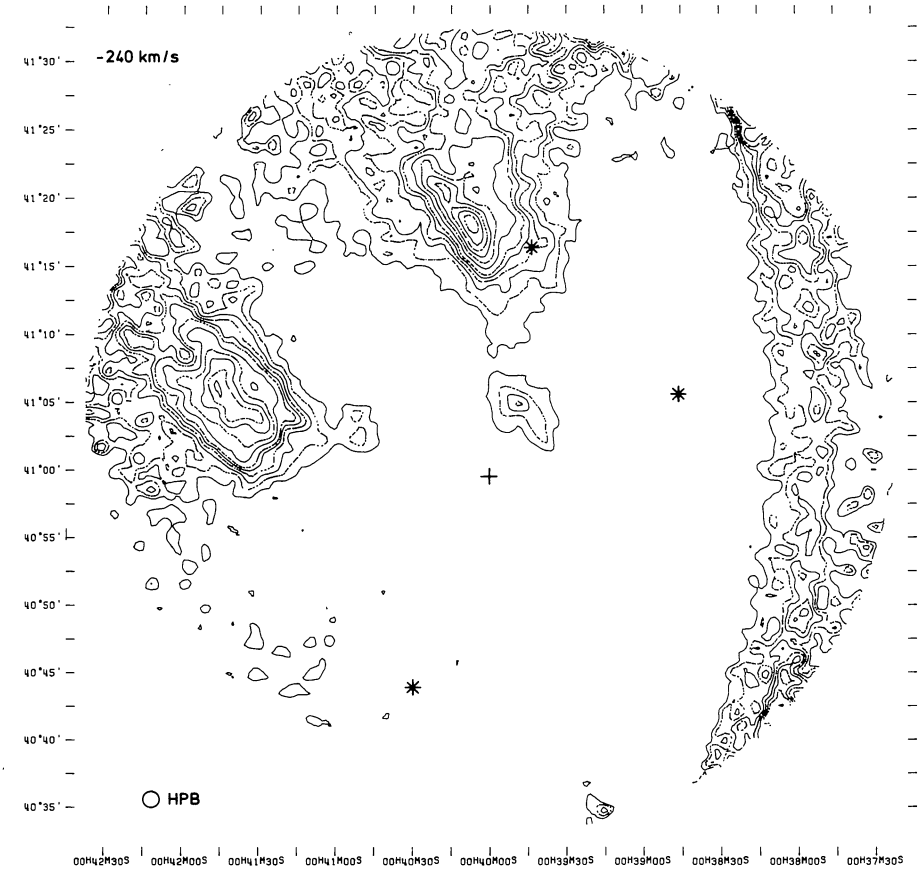

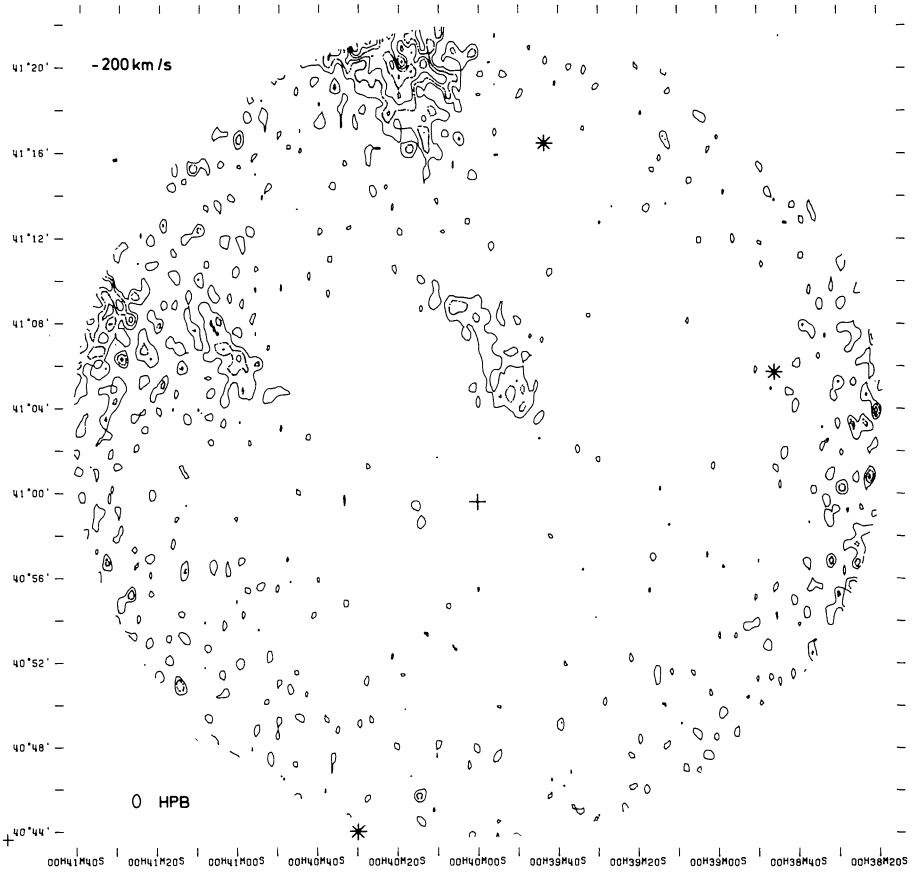

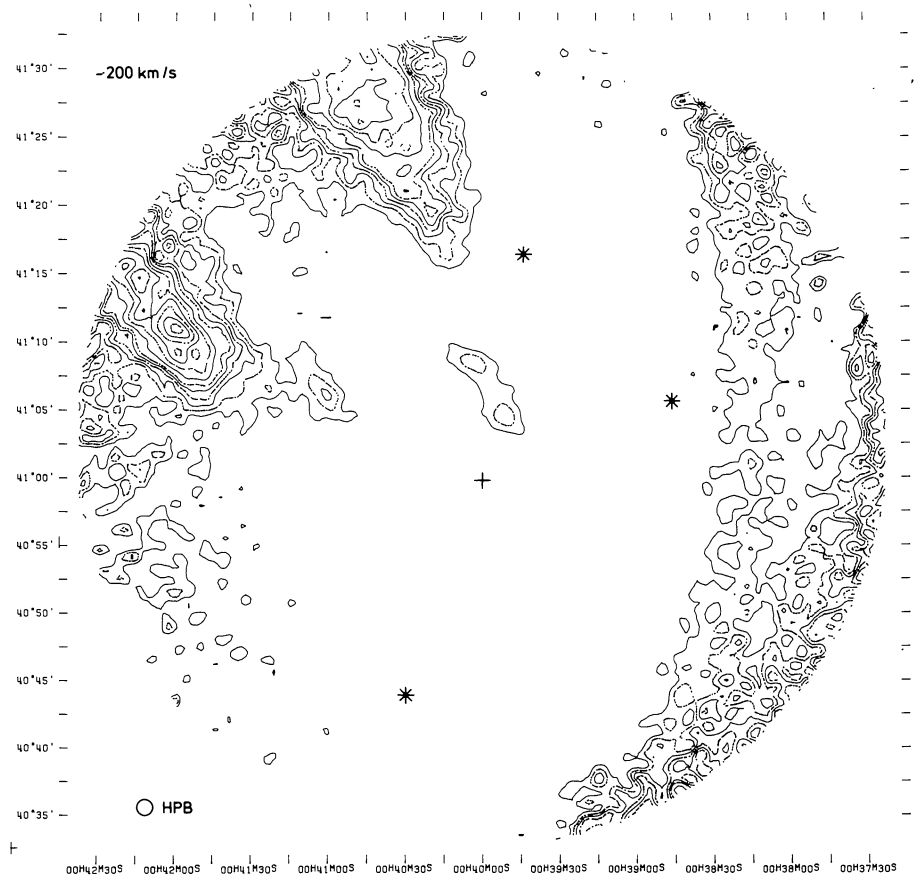

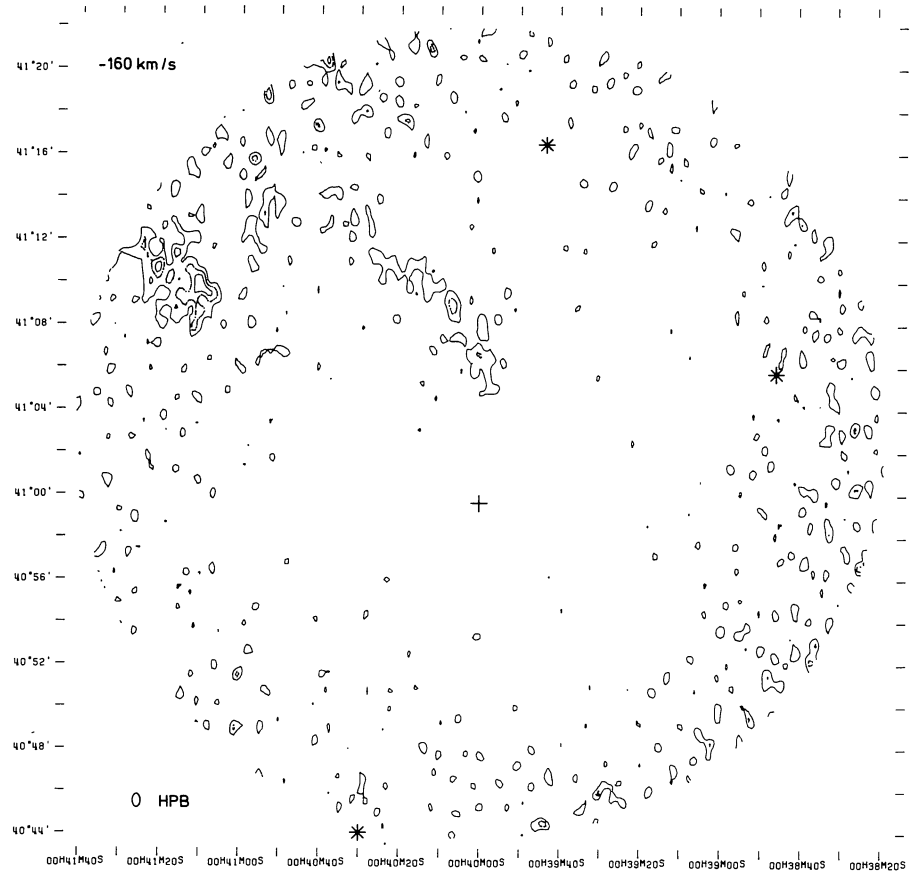

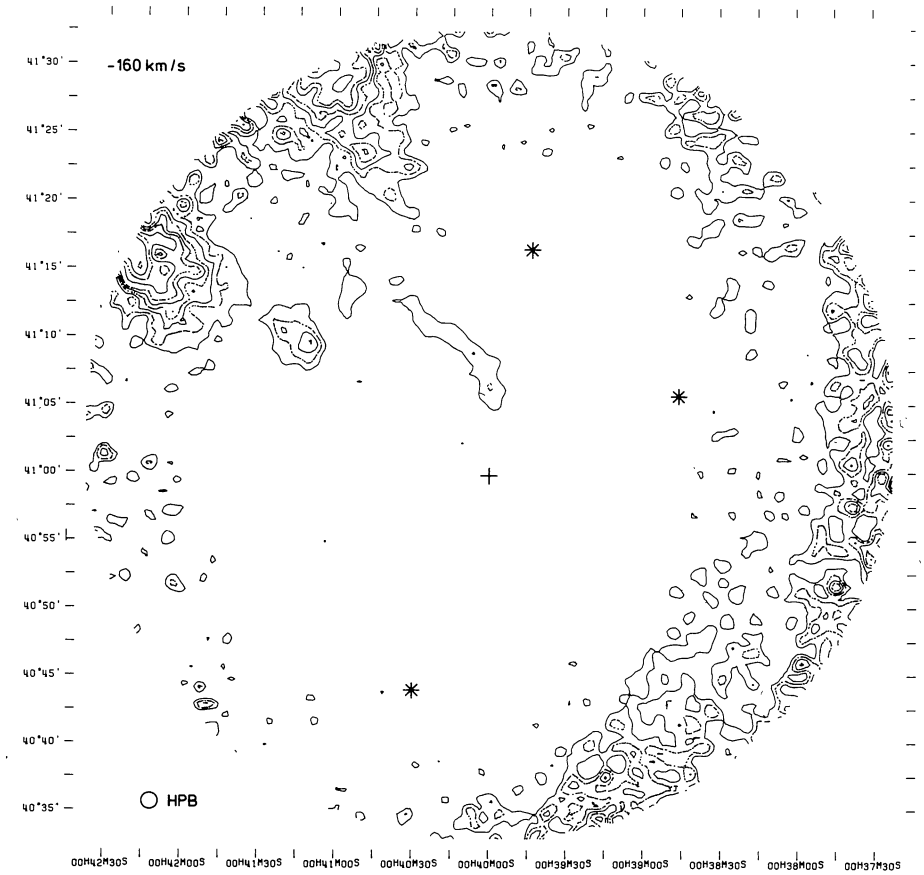

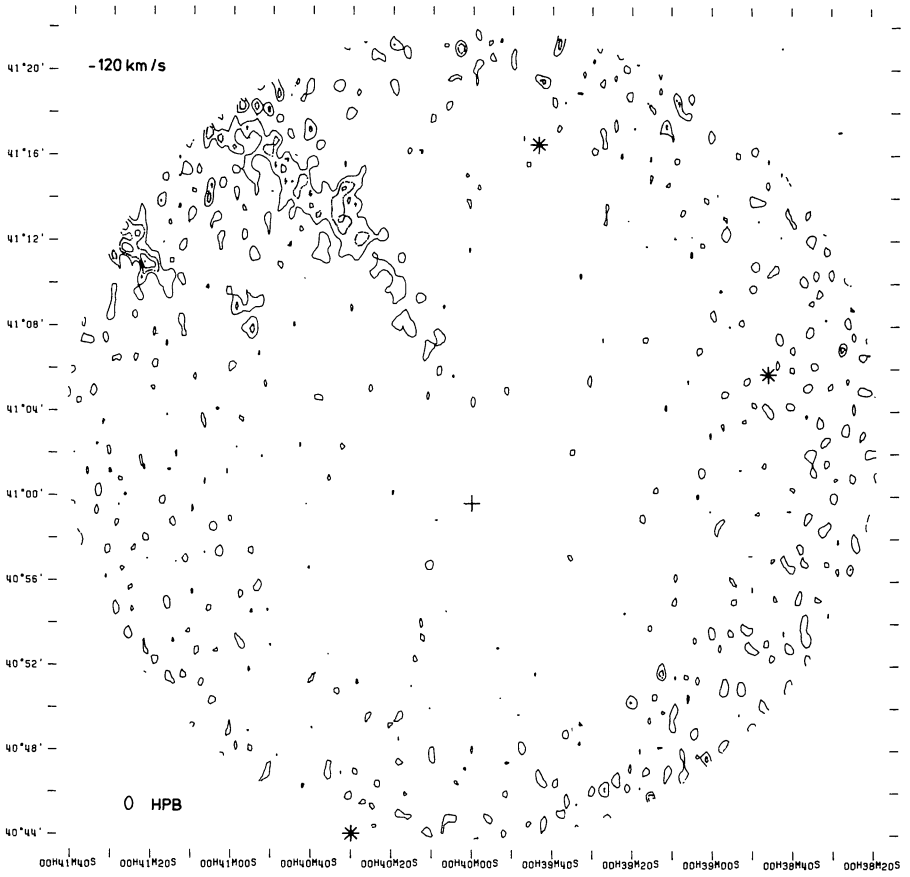

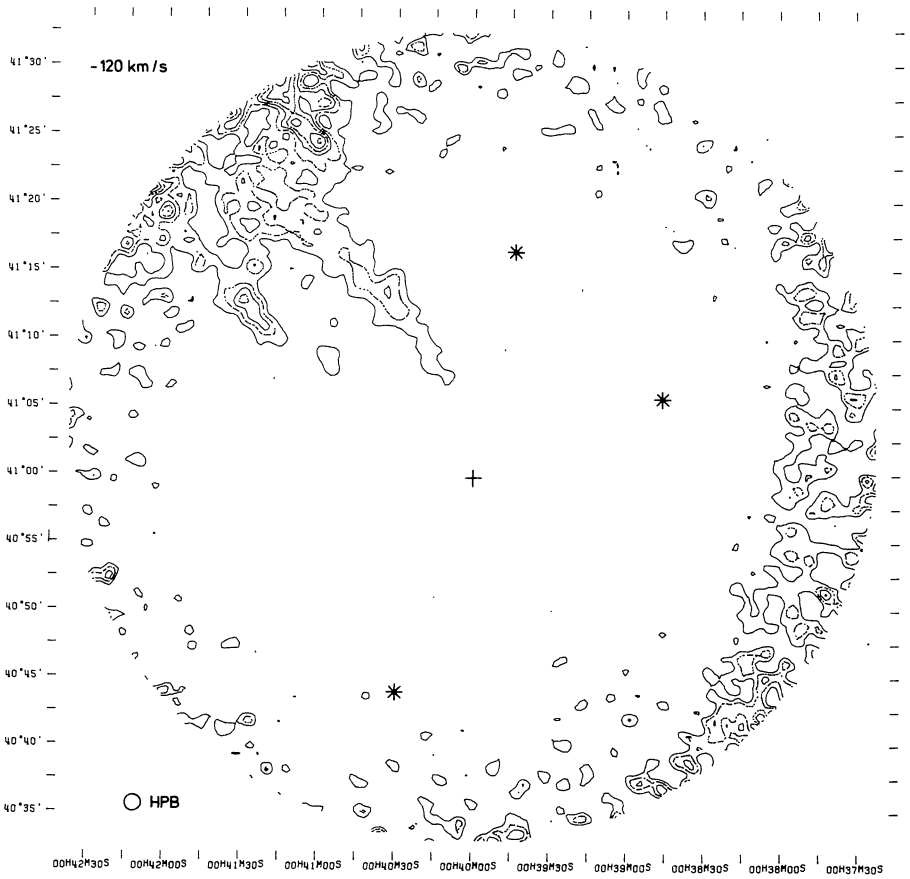

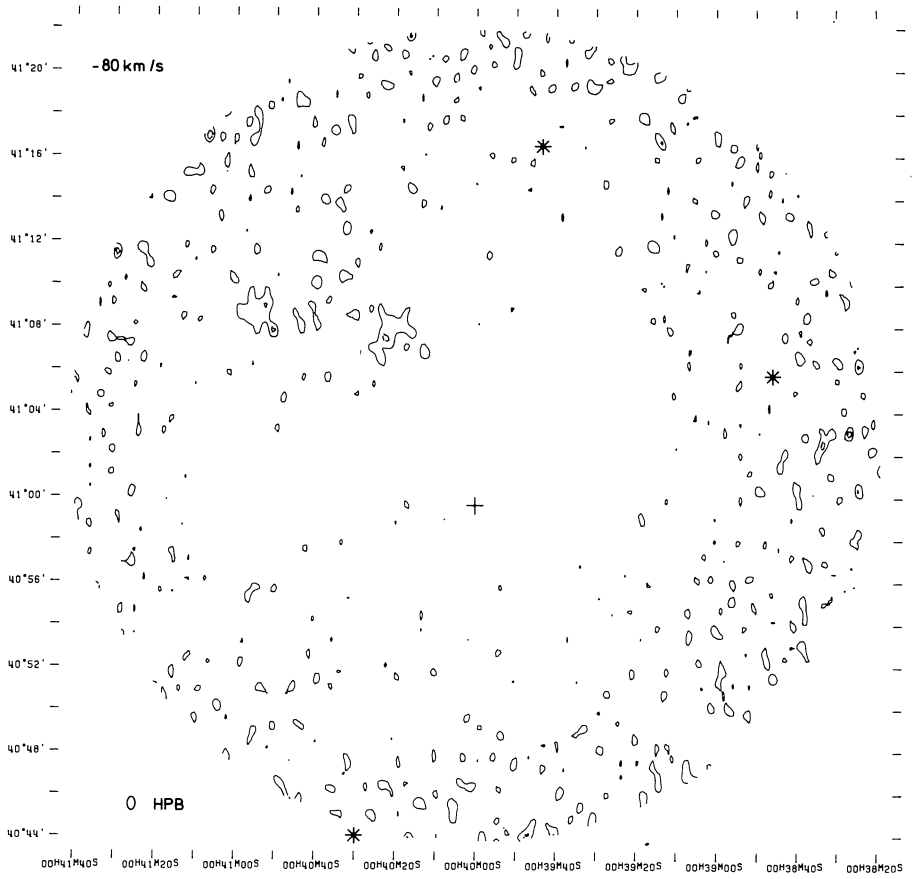

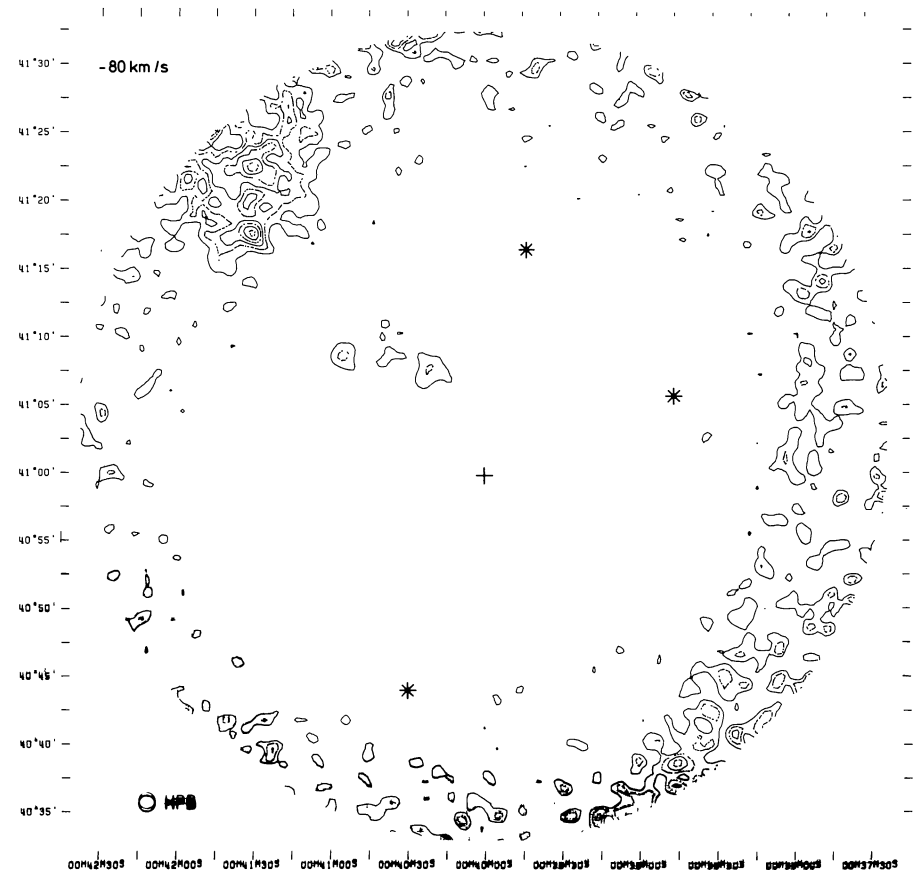

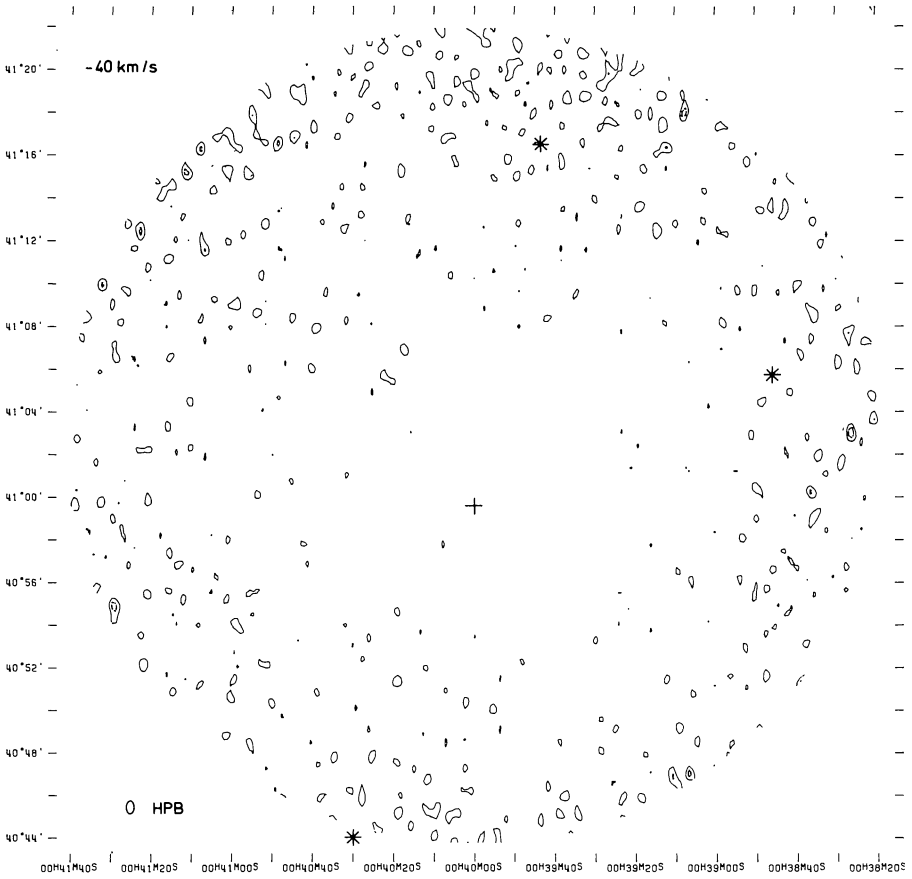

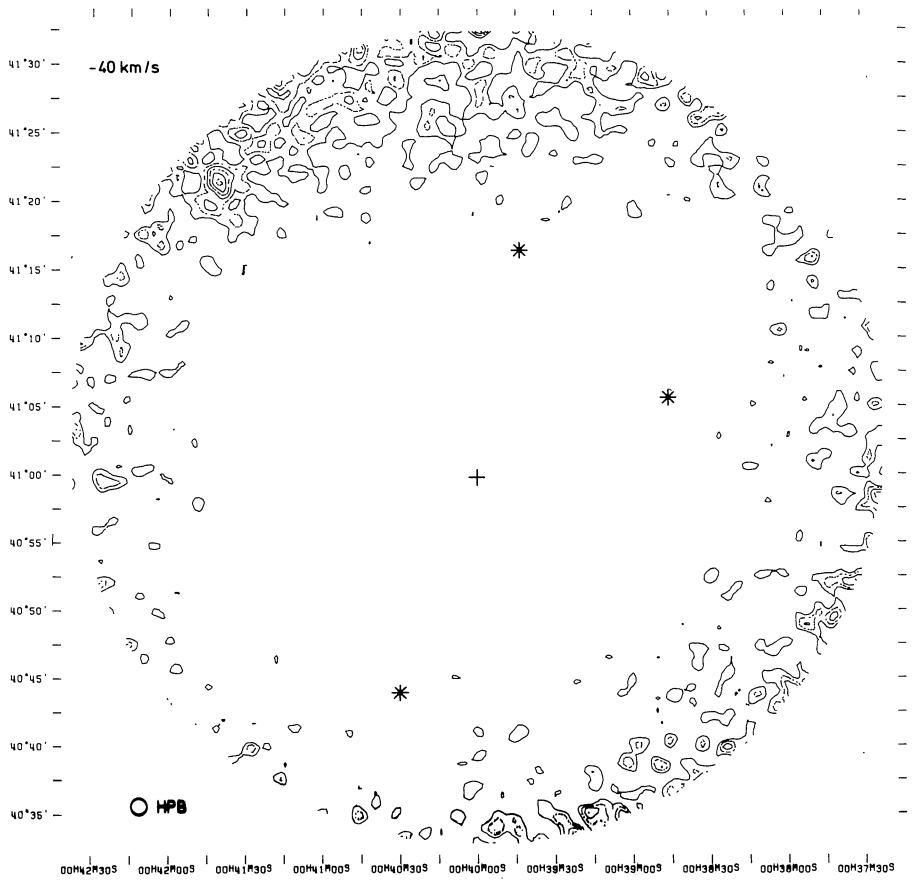

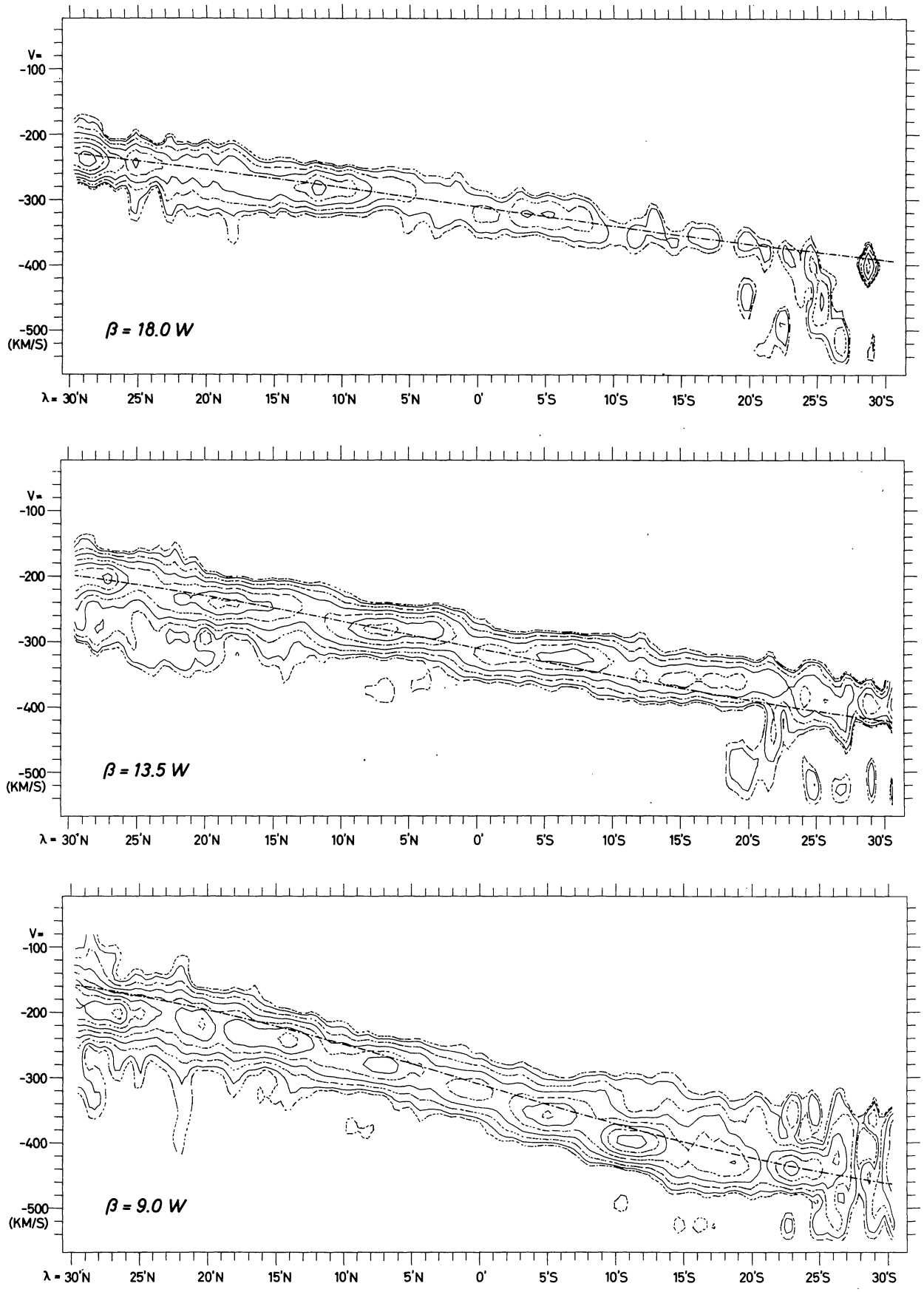

FIGURE 2. — Maps of 21-cm line brightness temperature as a function of position along the lines shown in figure 3 and of velocity. The expected velocity is plotted in each map as a heavy broken curve. The maps are further described in section 4.

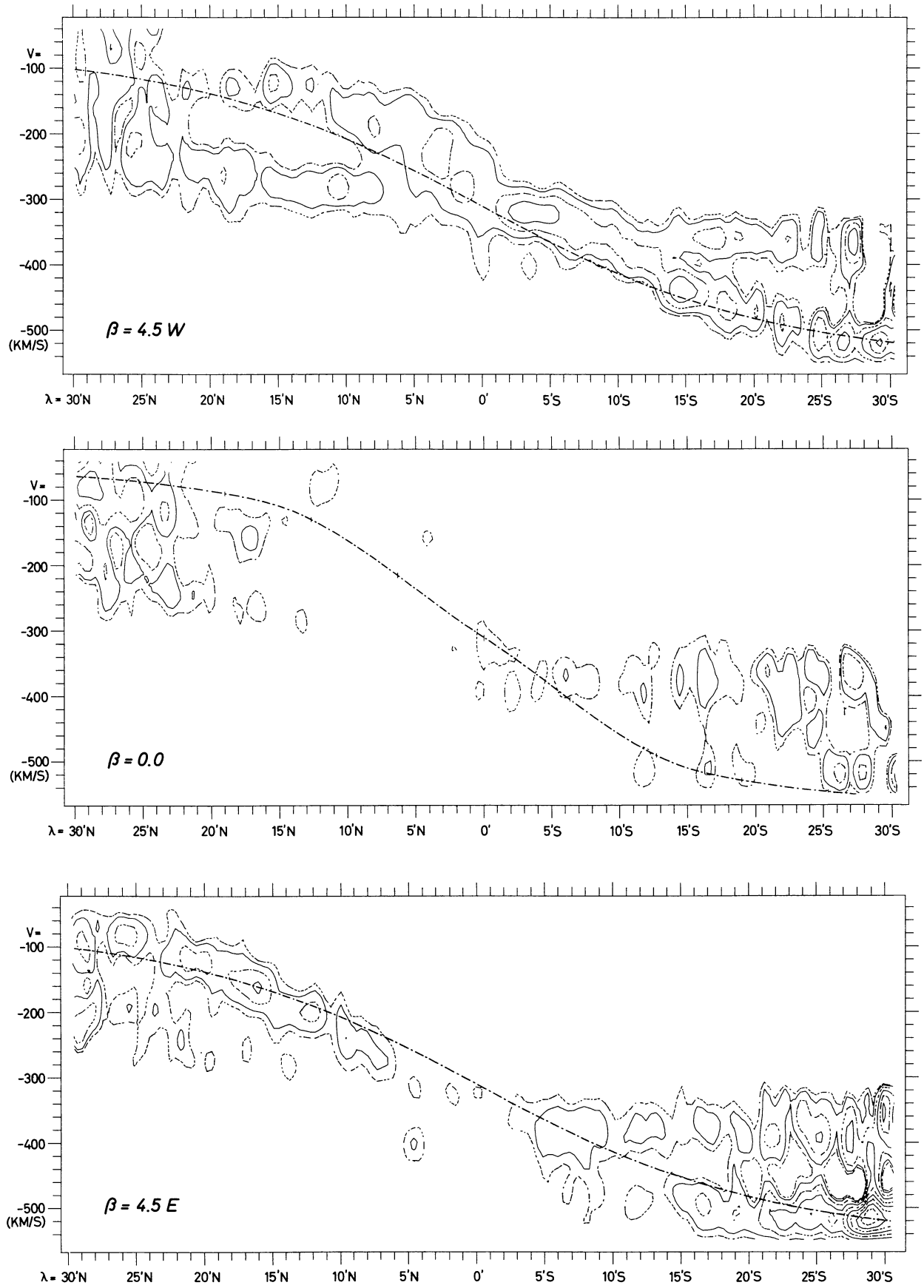

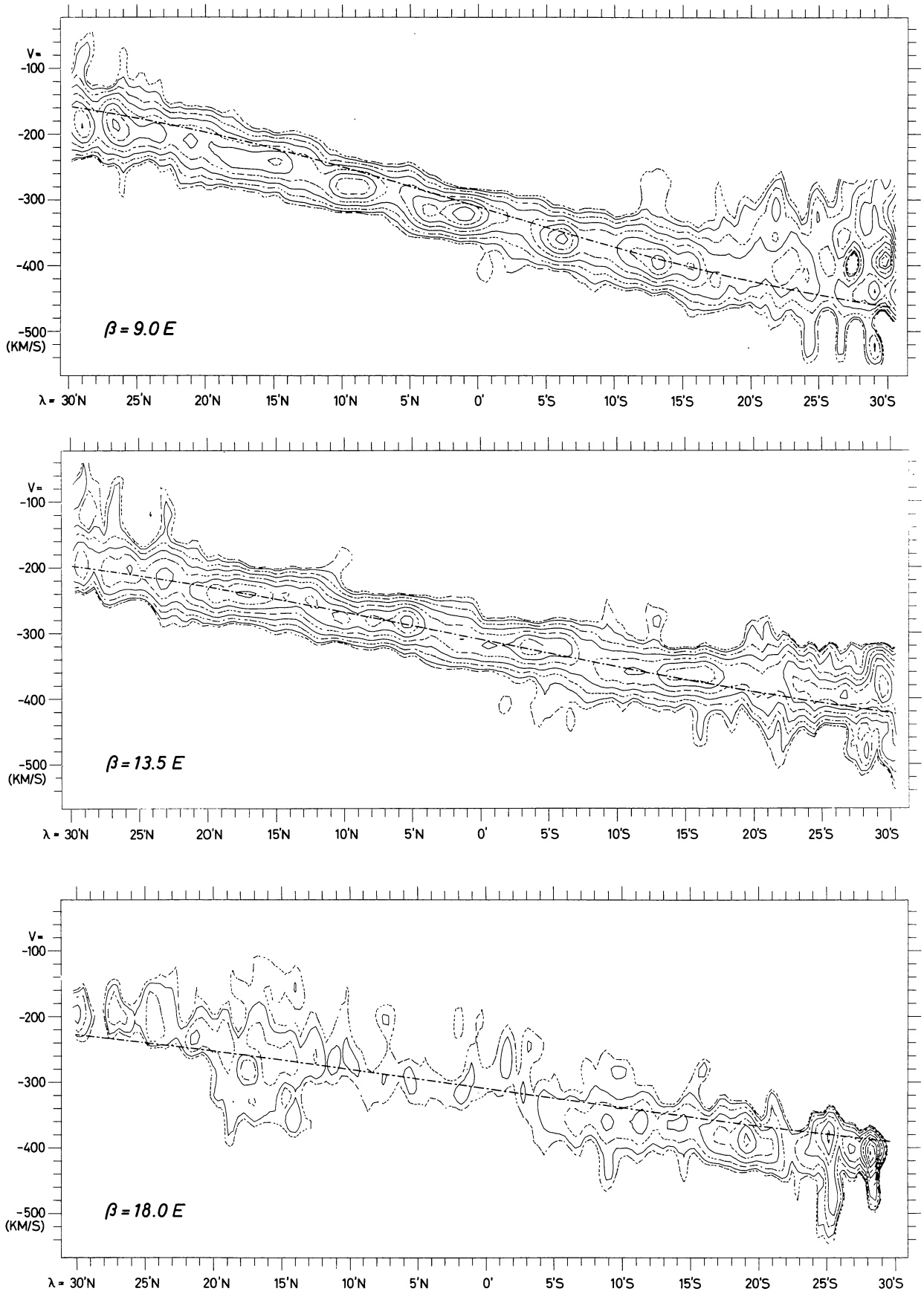

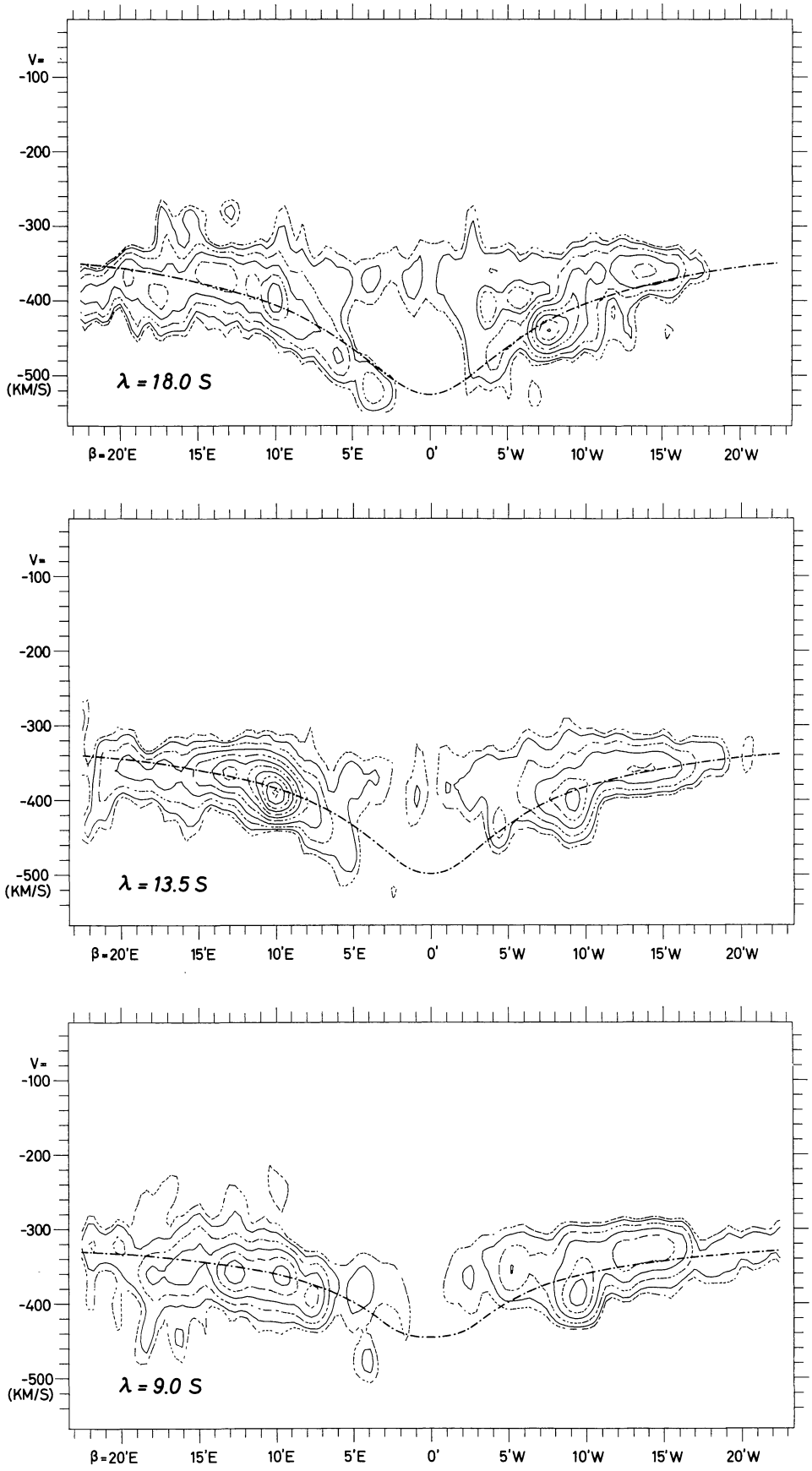

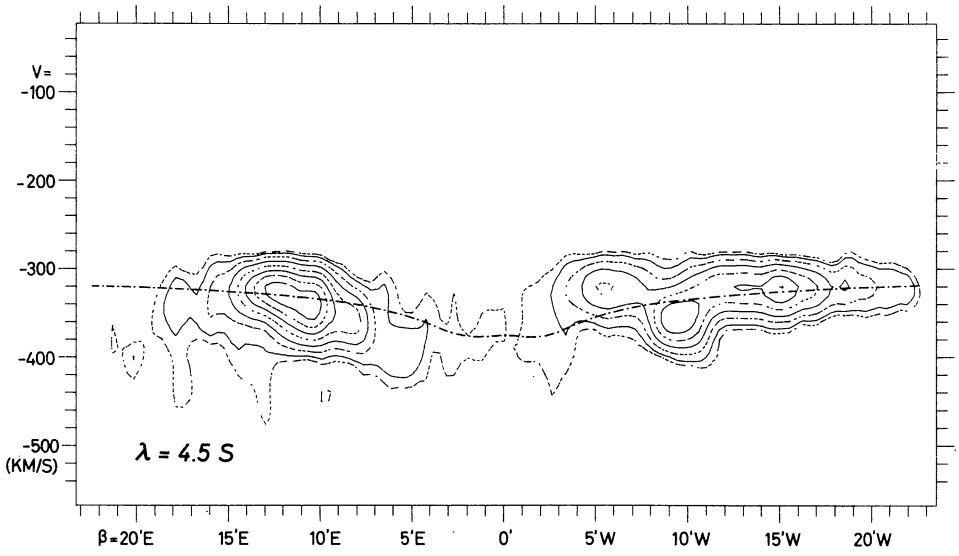

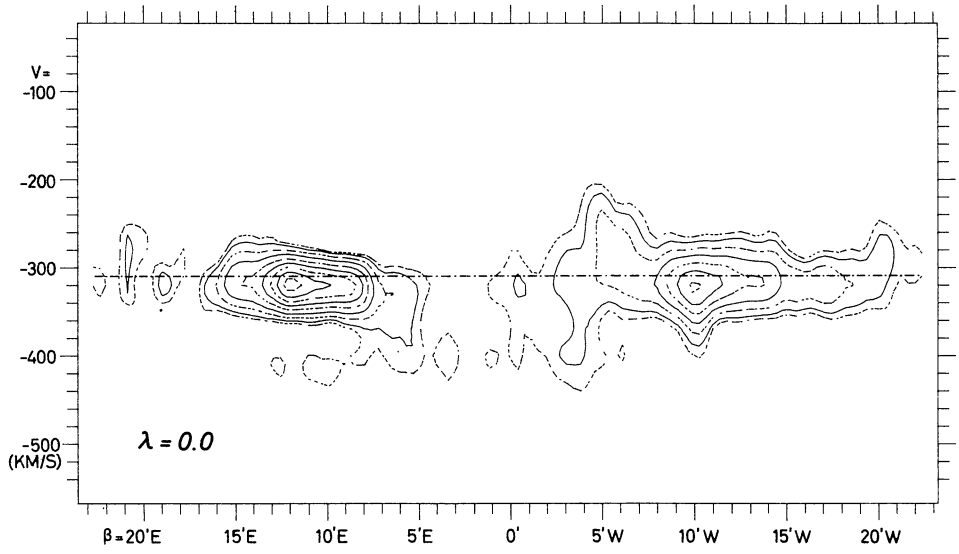

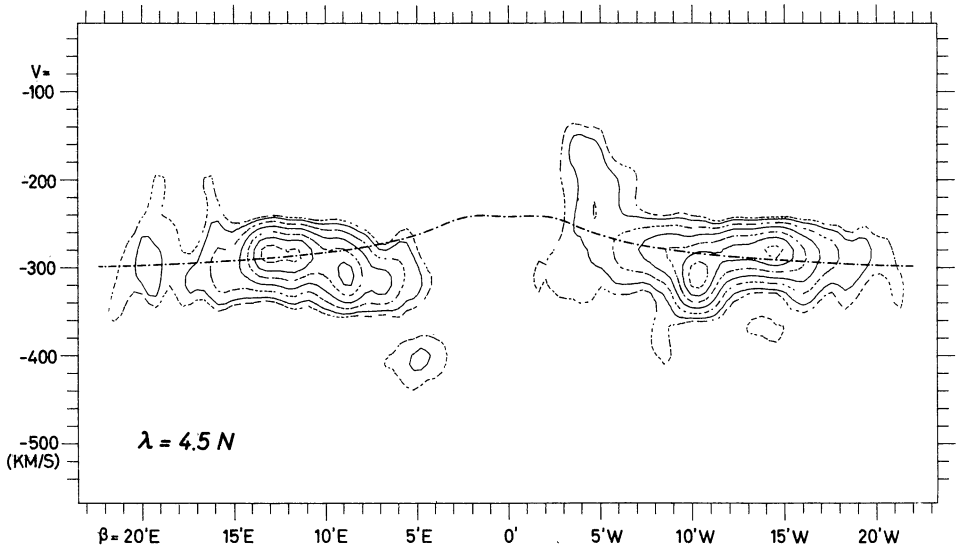

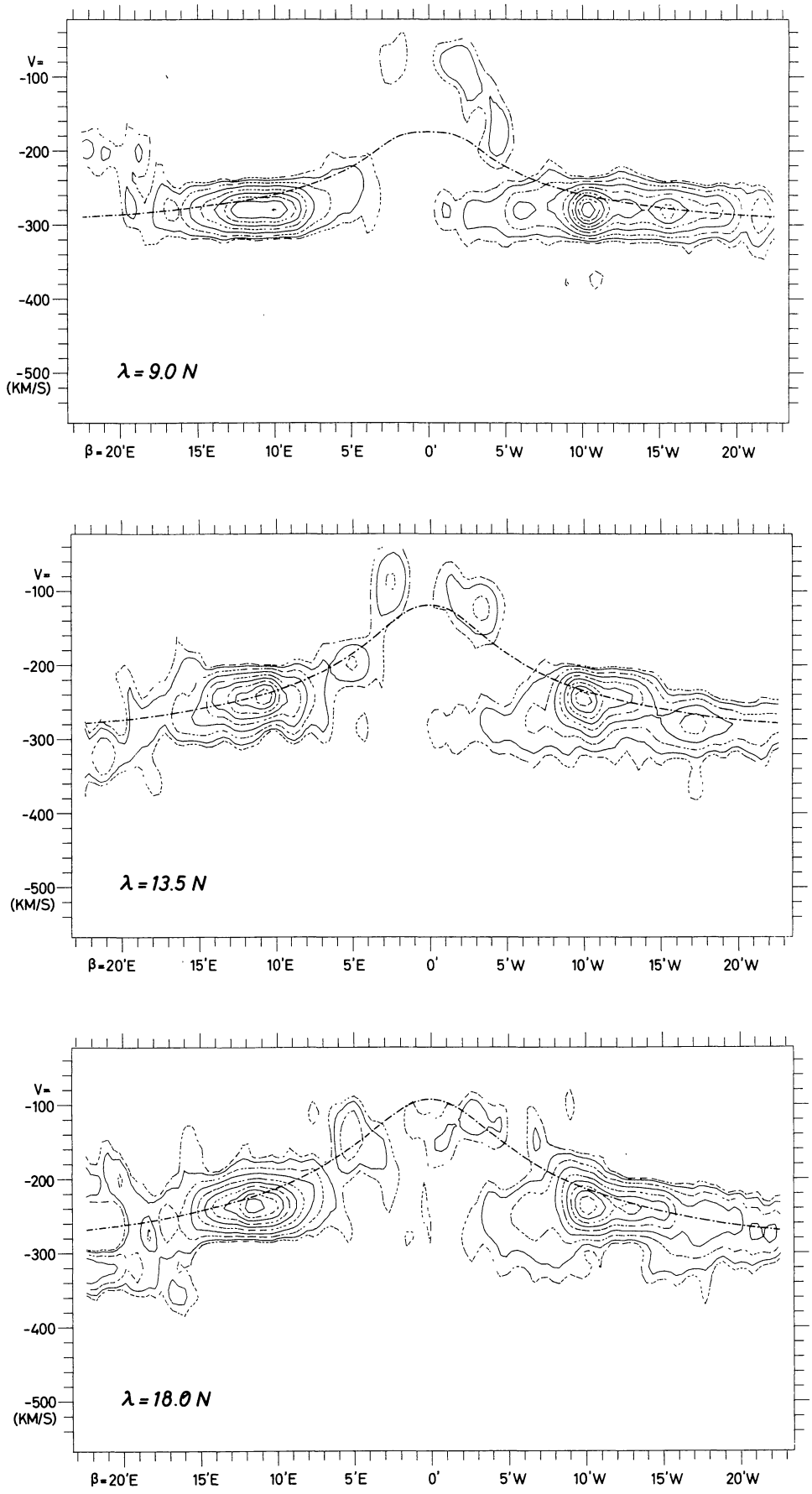

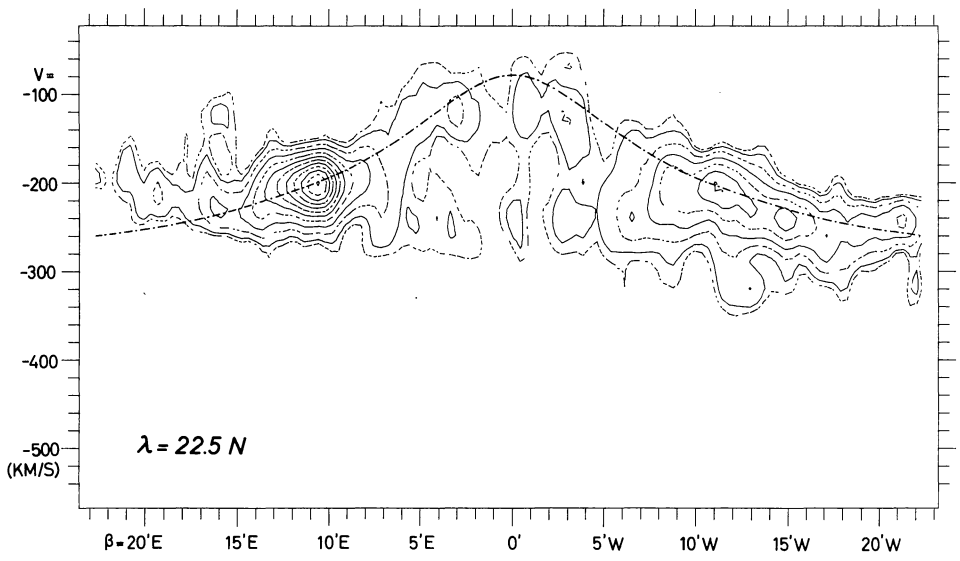

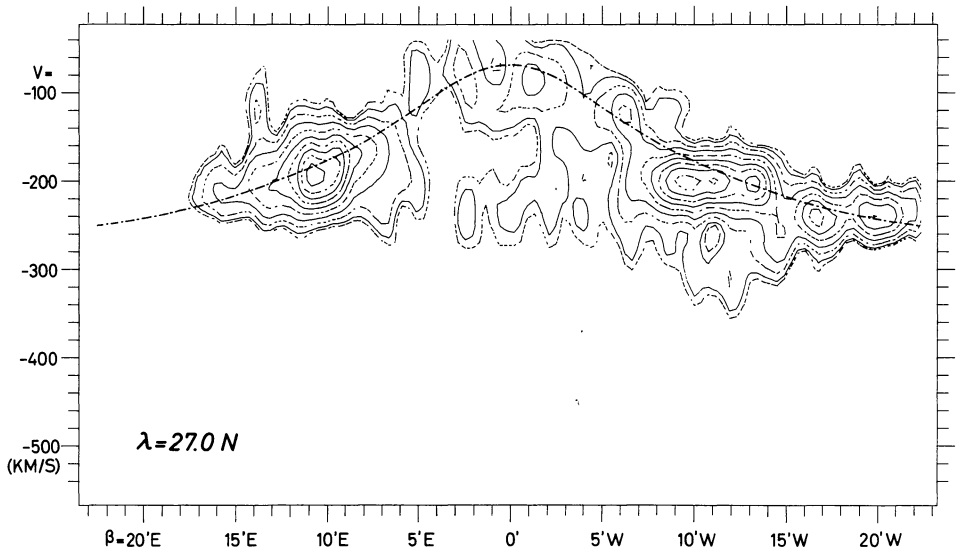

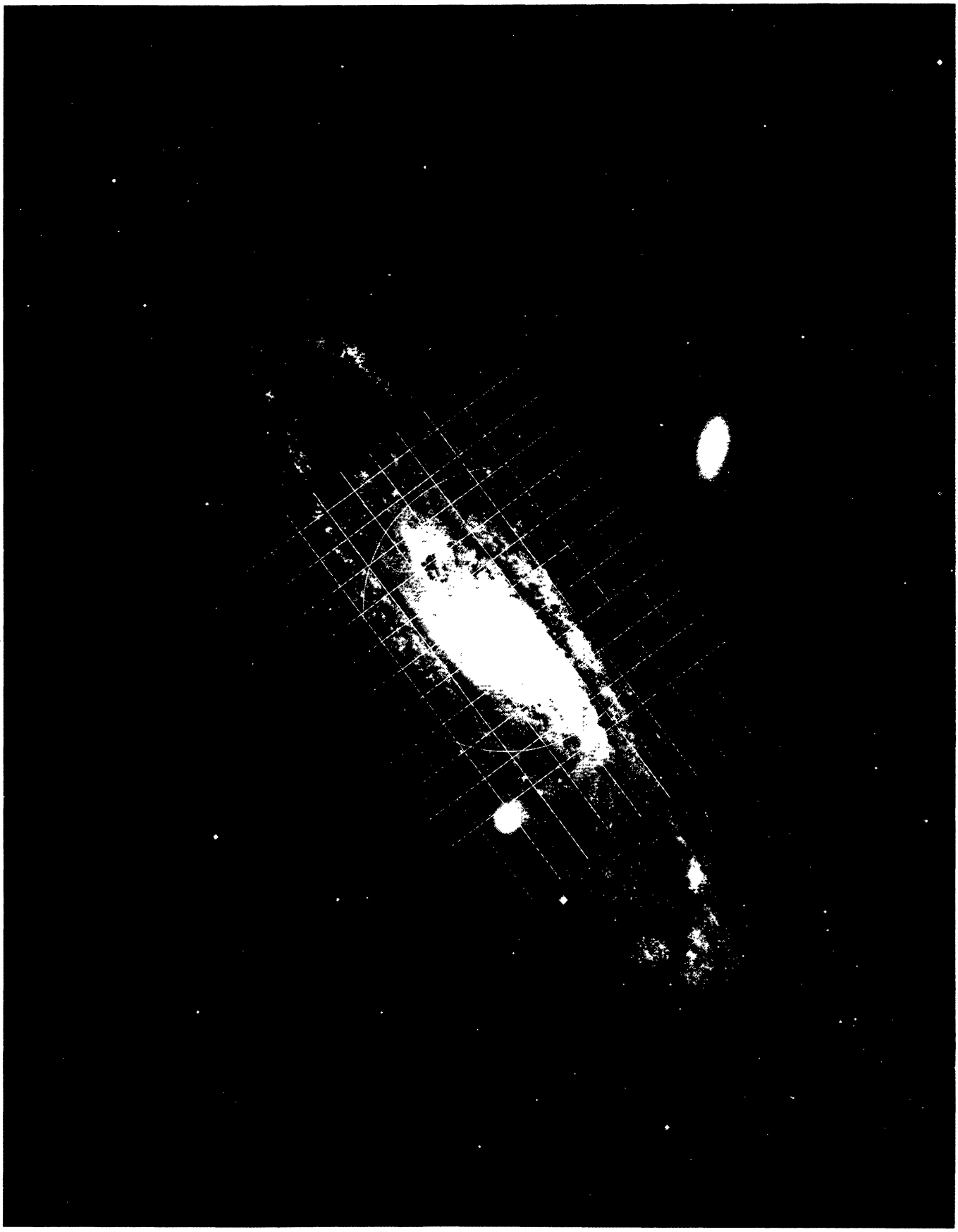

FIGURE 3. — Trajectories of the cross-cuts shown in figure 2 superimposed on a blue photograph of M31 (Palomar 48″ Schmidt photograph). The circle encloses the half-power primary beam.

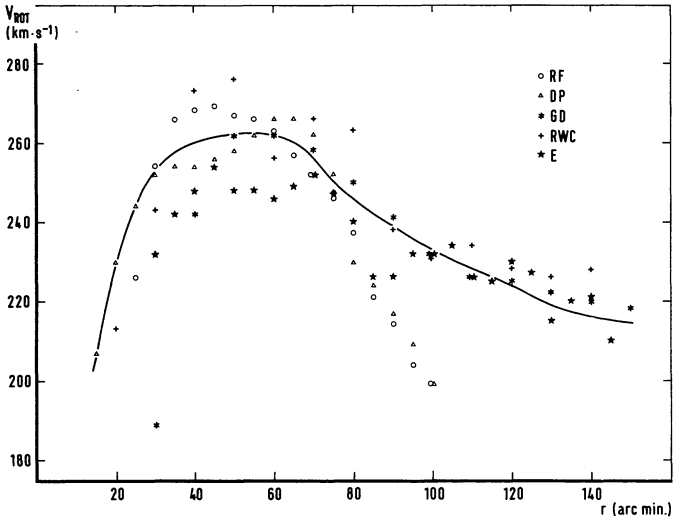

FIGURE 4. — The adopted rotation curve as described in section 5 and the observed points from the sources listed in table II. The extrapolation to the origin was by means of a smooth curve passing through the points (r = 12′, V_{rot} = 189 km s^{-1}), (9,139), (6,93) and (3,45).

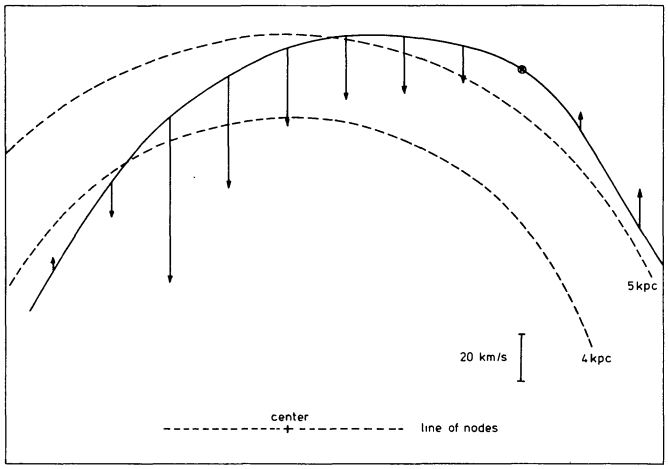

FIGURE 5. — Schematic map in the plane of M31 showing the position of arm 3 (solid line) and the line-of-sight components of the velocity deviation from the model (arrows).